THE UNIVERSITY OF OKLAHOMA

GRADUATE COLLEGE

FORCED CONVECTIVE HEAT TRANSFER AND THERMODYNAMICS IN THE SUPER CRITICAL REGION

A DISSERTATION

SUBMITTED TO THE GRADUATE FACULTY

in partial fulfillment of the requirements for the

degree of

DOCTOR OF PHILOSOPHY

BY

DONALD FINN

Norman, Oklahoma

1964

FORCED CONVECTIVE HEAT TRANSFER AND THERMODYNAMICS

IN THE SUPER CRITICAL REGION

APPROVED BY

Orin K. Crosser

C. M. Slepcevich

P. C. Hwang Yoon

Earl Eaton

DISSERTATION COMMITTEE

ACKNOWLEDGEMENT

The author wishes to express his sincere appreciation to the many individuals who have assisted in the experimental work and in the preparation of this dissertation. The following persons merit special mention for their invaluable assistance:

To Dr. O. K. Crosser, Associate Professor of Chemical Engineering, for his direction of this research and continued encouragement.

To Dr. C. M. Sliepcevich, Research Professor of Engineering, for his inspiration and advice.

To fellow graduate students Mr. K. A. Bishop and Mr. R. A. Sims for their assistance in electronic equipment design and construction.

To Mr. S. M. Moffez for his help in equipment construction and data collection.

Finally to the author's wife, Elaine, who has assisted in the preparation of this dissertation and whose continued encouragement made this endeavor possible.

In conclusion, the author wishes to thank the National Science Foundation for their financial assistance and the University of Oklahoma Computing Laboratory for their help in computational phases of the research.

ABSTRACT

An apparatus was constructed for the determination of thermodynamic properties and convective heat transfer coefficients for propane in the supercritical region. Propane was circulated through a closed heat transfer loop containing an electrically heated, horizontal, 0.3 inch I.D. Inconel tube. The tube served as a flow calorimeter to measure specific enthalpy changes at 700 psia as a function of the inlet and exit bulk fluid temperatures in the range 165 - 250F. The enthalpy-temperature behavior was constructed by a least squares computer fit utilizing the Schmidt orthogonalization algorithm. The data are believed accurate to 0.5 Btu/lbm. The isobaric heat capacity was calculated from the enthalpy data. The thermodynamic results are tabulated and presented graphically as a function of temperature. Calorimetric data were not previously available for propane in this region.

Heat transfer coefficients were determined from measurements of the wall temperature profile and heat flux, and calculations of the bulk fluid temperature at various positions along the tube. The range of variables studied was:

Reynolds Number: 80,000 to 800,000
Heat transfer rate: 10,000 to 120,000 Btu/hr.sq.ft.
Bulk fluid temperature: 165 - 250F

The experimental coefficients exhibited normal behavior. After entrance effects, the heat transfer coefficients increased, decreased, or remained essentially constant with length depending primarily on whether the ratio of the wall-to-bulk specific heat capacities was greater than, less than, or approximately unity. Relative maximums were observed in the heat transfer coefficients as a function of bulk or wall temperature at constant heat flux and Reynolds number. The relative maximums became smaller and less pronounced and were displaced further from the transposed critical temperature as the heat flux was increased.

An expression for the heat transfer coefficient is proposed which represents an extension of Petukhov's equation to account for density effects:

$$h = h'_{t_b} \left(\frac{C_{pm}}{C_{pb}} \right)^{0.54} \left(\frac{k_b}{k_w} \right)^{0.20} \left(\frac{\rho_b}{\rho_w} \right)^{0.27} \left(\frac{\mu_b}{\mu_w} \right)^{0.02}$$

This equation correlates successfully local heat transfer coefficients for propane in the supercritical region. The correlation reduces to the conventional expression when applied to regions where property variations are small and yields conservative estimates in the near transposed critical state.

TABLE OF CONTENTS

LIST OF TABLES

LIST OF ILLUSTRATIONS

FORCED CONVECTIVE HEAT TRANSFER AND THERMODYNAMICS IN THE SUPER CRITICAL REGION

CHAPTER I

INTRODUCTION

With the development of equipment for heat transfer at extreme operating temperatures and pressures, the problem of variable fluid properties has become more severe. Large temperature differences between the fluid and the contact surface at ordinary conditions can cause a severalfold change in the physical and thermodynamic properties. However, as long as these variations are uniform, the usual empirical or semitheoretical correlations using constant or reference state properties have generally been successful in predicting the heat transfer characteristics. When the property variations are both irregular and large, such as occurs in the critical region of a fluid, the conventional correlating techniques have not been successful.

The major objective of this investigation was to study forced convection heat transfer in the supercritical region and to develop a method of correlating the results so that predictions might be made without heat transfer measurements. Propane, whose critical point occurs at 206.3F and

617.4 psia, was selected for study for two reasons: (1) the ease of attaining the critical state without adverse effects due to high pressures and temperatures, and (2) the availability of physical property data for the critical region.

In addition to the physical properties, viscosity, thermal conductivity and density, it is necessary to have an accurate knowledge of the specific enthalpy or isobaric heat capacity in order to determine the accuracy of the results and to study the effect of property variations on the heat transfer coefficient. In the critical region, these thermodynamic data are either non-existent for most fluids or they have been calculated from volumetric data, and as such, are subject to large errors. Hence, the apparatus was constructed to operate as a flow calorimeter in order to measure the thermodynamic properties of propane.

The experimental method consisted of measuring the energy transferred to propane flowing turbulently through an electrically heated Inconel tube, 0.358 in. outside diameter, 0.0285 in. wall thickness, and 21 in. long. The variables measured were: (1) bulk fluid temperatures at inlet and outlet, (2) mass flow rate, (3) electrical power dissipation or heat flux, (4) static fluid pressures, (5) pressure drop across the tube, and (6) the external wall temperature profile as a function of tube length. A local rather than an average heat transfer coefficient was determined because of property variations and entrance effects. The coefficient was defined by the expression:

$$h = \frac{q_w}{t_w - t_b} \qquad (1)$$

where:

q_w = local rate of heat transfer per unit inside wall area

t_w = inside wall temperature

t_b = bulk fluid temperature

The problem of heat transfer in the critical region has at least two important aspects. These are: (1) the effect of variable fluid properties on the rate of transport and (2) the effect of the proximity to the critical state on the transport mechanism. The present investigation is a study of these problems.

CHAPTER II

SURVEY OF THE LITERATURE

Heat Transfer Correlations

Most empirical and semitheoretical correlations for convective heat transfer attempt to correlate the heat transfer coefficient in terms of dimensionless groupings of the variables characterizing the geometry and fluid properties. A typical example of such correlations is

$$Nu = a\ Re^b\ Pr^c \qquad (2)$$

where

Nu = Nusselt number, hD/k

Re = Reynolds number, DG/μ

Pr = Prandtl number, $C_p\mu/k$

a,b,c = constants

These correlations have not been successful in the critical region. This is probably due to the rapid and irregular variation of the physical and thermodynamic properties with temperature so that it is difficult to decide what value to use for these properties in the correlation. Deissler (7) has proposed a reference temperature rule for evaluating the Nusselt and Reynolds numbers which he formulated from

calculated Nusselt numbers for supercritical water. Bringer and Smith (5) have tested this rule on experimental heat transfer data for carbon dioxide at 1200 psia. They found that the correlation did not fit their data.

Other workers (15,19,32,36, and 40) have suggested the use of reference temperatures. Utilizing both theoretical and experimental results, Rubesin and Johnson (32), and later Eckert (15), Sommer and Short (36) and Young and Janssen (40) found that heat transfer correlations with constant properties could be applied to cases with property variation if the properties were evaluated at an appropriate reference temperature. These studies were concerned with both laminar and turbulent boundary layer flow across flat plates. Knuth (20, 21) has extended the analysis further with considerable success except for certain types of chemical reactions (19). The study of reacting systems was more pertinent to studies in the near-critical region because these systems have high effective heat capacities. However, the variation of heat capacity with temperature in all these studies was never so large or irregular as the variation in the critical region. Because the reference state procedures have been successful only with small or uniform changes in properties, it would appear doubtful that such an approach would be successful in the near-critical region.

Shitzman (35) has presented a dimensionless correlation in the form of Equation (2). The Reynolds and Nusselt numbers are calculated using physical properties evaluated at

the bulk fluid temperature. The Prandtl number is taken as the smaller of the values computed at the wall and bulk temperature. Koppel and Smith (23) applied Shitzman's correlation to their data and those of Bringer and Smith (5), Dickinson and Welch (13), and Powell (30). The correlation was not satisfactory on a Shitzman type plot.

Deissler (7,8,9,10,11) has proposed a model for the calculation of temperature and velocity profiles for turbulent heat transfer to fluids with variable physical properties. This model is based on the anology between heat and momentum transfer. The following equations for the rates of momentum and heat transfer perpendicular to the direction of flow have been used by Deissler to predict semitheoretical expressions for the heat transfer coefficients :

$$\tau = \frac{1}{g_c} (\mu + \rho\epsilon_m) \frac{du}{dy} \tag{3}$$

$$q = -(k + \rho C_p \epsilon_h) \frac{dt}{dy} \tag{4}$$

where:

τ = shear stress

μ = bulk viscosity

ρ = density

ϵ_m = eddy diffusivity of momentum transfer

u = local fluid velocity

y = perpendicular distance from wall

q = rate of heat transfer per unit area

k = thermal conductivity

C_p = isobaric heat capacity

ϵ_h = eddy diffusivity of heat transfer

g_c = dimensional constant

t = local fluid temperature

Deissler defined dimensionless velocity, temperature and distance variables,

$$u^+ = \frac{u}{v_*} \tag{5}$$

$$y^+ = \frac{v_* \, y}{\mu_w/\rho_w} \tag{6}$$

$$t^+ = \frac{(t_w - t)\rho_w C_{pw} v_*}{q_w} = \frac{1}{\beta}\left(1 - \frac{1}{t_w}\right) \tag{7}$$

$$v_* = \left(\frac{g_c \tau_w}{\rho_w}\right)^{1/2} \tag{8}$$

which upon substituting into Equations (3) and (4) yield:

$$\frac{\tau}{\tau_w} = \left[\frac{\mu}{\mu_w} + \frac{\rho}{\rho_w}\frac{\epsilon_m}{\mu_w/\rho_w}\right]\frac{du^+}{dy^+} \tag{9}$$

$$\frac{q}{q_w} = \left[\frac{k}{k_w Pr_w} + \frac{\rho C_p}{\rho_w C_{pw}}\frac{\epsilon_h}{\mu_w/\rho_w}\right]\frac{dt^+}{dy^+} \tag{10}$$

where the subscript w denotes conditions at the wall; the superscript +, dimensionless variables; and β is the dimensionless heat transfer parameter defined by Equation (7).

In order to integrate Equations (9) and (10) to obtain the velocity and temperature profiles across the tube, Deissler assumed:

(1) The eddy diffusivities of momentum and heat are equal and are given by:

$$\frac{\epsilon}{\mu_w/\rho_w} = n^2 u^+ y^+ \left[1 - \exp\left(-\frac{n^2 u^+ y^+}{\mu/\mu_w}\right)\right] ; \; y^+ \leq 26 \tag{11}$$

$$\frac{\epsilon}{\mu_w/\rho_w} = \frac{m^2 \left(\frac{du^+}{dy^+}\right)^3}{\left(\frac{d^2u^+}{dy^{+2}}\right)^2} ; \quad y^+ > 26 \tag{12}$$

where m and n are experimentally determined constants.

(2) The variation in the shear stress and the heat transfer rate across the tube has a negligible effect on the velocity and temperature profiles, i.e., τ/τ_w and q/q_w are unity.

(3) The physical and thermodynamic properties may be represented by a logarithmic relationship of the form:

$$\psi/\psi_w = a(1 - \beta t^+)^b \tag{13}$$

where:

$\psi = \mu$, ρ, C_p, or k

a,b = constants, different for each property

With these three assumptions, Deissler solved Equations (9) and (10) simultaneously by iteration to obtain the velocity and temperature profiles. The profiles were then integrated to give the bulk temperature and velocity which were used to

calculate the heat transfer coefficient from Equation (1). Deissler (10) has presented results for supercritical water in the form of a Nusselt-Reynolds number plot with various parameters of β at constant wall temperature and pressure.

Deissler's model has been fairly successful in predicting Nusselt numbers. The solution, however, involves lengthy iterative calculations and hence is limited to use with high speed computers. It is also based on the assumption of constant heat flux and shear stress, assumption (2). Calculated evidence indicates that the variation of shear stress and heat flux with radial position does not significantly affect the profile. It would appear, however, that the accuracy of this supposition could be justified only on the basis of experimental velocity and temperature measurements.

Hsu and Smith (18) have modified Deissler's expression for the eddy diffusivity to account for the effect of density variation. Their results show that the density effect improved the agreement with the experimental data of Bringer and Smith (5).

Goldmann (16) has developed a theoretical analysis of turbulent heat and momentum transport with variable fluid properties. His analysis differs from Deissler's in that the coefficients in the expressions for the eddy diffusivity are assumed variable. Goldmann defines a turbulence damping function which he determines from Deissler's calculated universal velocity profile. He integrates simultaneously the radial transport equations, (3) and (4), to obtain the

velocity and temperature distributions. These integrations are also subject to the assumption of constant radial shear stress and heat flux. The results are, however, only slightly different than those of Deissler.

Dickinson and Welch (13) have measured heat transfer coefficients for supercritical water at 3500 and 4500 psia. They obtained film conductances greater than those predicted by either Deissler's or Goldmann's analysis. The heat transfer coefficients were correlated as a function of the wall temperature.

Visual observations by Griffith and Sabersky (17), of free convective heat transfer from a hot wire to Freon 114A, tend to confirm a boiling-like mechanism for heat transfer at supercritical pressures under certain conditions. Goldmann (16) first postulated a boiling-like mechanism in his discussion of Deissler's paper (7). He surmised that ". . . macroscopic clusters of liquid-like molecules 'explode' at the heat-transfer surface, move as gaslike aggregates into the bulk of the fluid where they 'collapse' again into liquidlike clusters. One may speculate that the growth and collapse of these clusters, like the growth and collapse of bubbles during boiling at subcritical pressures, cause enough agitation to result in heat transfer coefficients that are significantly higher than predicted in the paper (Deissler's)."

Powell (30) has investigated supercritical heat transfer to oxygen and nitrogen in a vertical electrically heated tube. Under certain conditions, he observed a "hot-spot", a

region of the tube which attained a much higher temperature than the rest of the wall. The "hot-spot" seemed to occur when the bulk fluid temperature approached the transposed critical temperature. The transposed critical temperature is defined as the temperature at which the isobaric specific heat capacity is a maximum. Powell was able to move the "hot-spot" up and down the tube by changing the location of the transposed critical temperature. No explanation has been found for this unusual phenomena.

Perhaps the first practical problem in which physical property variations were severe was in the heating and cooling of viscous petroleum fractions where the viscosity change was large. An empirical modification, using the wall-to-bulk viscosity ratio was successfully introduced by Sieder and Tate (34) to correct the conventional correlation. Petukhov, Krasnoschekov, and Protopopov (28) recently extended the empirical approach to account for other property variations in addition to viscosity. They obtained the expression,

$$Nu_b = Nu_b' \left(\frac{C_{pm}}{C_{pb}} \right)^{0.35} \left(\frac{k_w}{k_b} \right)^{0.33} \left(\frac{\mu_b}{\mu_w} \right)^{0.11} \qquad (14)$$

where:

$$C_{pm} = \frac{\overline{H}_w - \overline{H}_b}{t_w - t_b} \qquad (15)$$

$\overline{H}$ = specific enthalpy

b = subscript, denoting bulk fluid conditions

from the analysis of their data together with test data of

other investigators on heat transfer to supercritical carbon dioxide (5) and water (13,25, and 35). In all, 720 experimental points were correlated, including 307 for carbon dioxide. Approximately 90% of the correlated data was within ±20% of the value predicted by Equation (14). The isothermal bulk Nusselt number, Nu_b', was given by the expression of Petukhov and Kirilov (27),

$$Nu_b' = \frac{Re_b \, Pr_b \, \frac{f_b}{2}}{12.7 \left(\frac{f_b}{2} \right)^{1/2} (Pr_b^{2/3} - 1) + 1.07} \qquad (16)$$

where f_b is the friction factor defined as

$$f_b = \frac{2 \, g_c \, \tau_w}{\rho_b \, v^2} \qquad (17)$$

Physical and Thermodynamic Properties

The experimental determination of the heat transfer coefficient by the method used in this investigation required knowledge of the pressure-temperature behavior of the specific enthalpy and fluid density. In addition to these variables, it was also desirable to have similar information for the thermal conductivity, viscosity, and the isobaric heat capacity, in order to determine the effect of property variations on the heat transfer coefficient.

The variation of thermal properties in the critical region has been well established by numerous investigators. However, recent measurements of the transport coefficients,

i.e., viscosity and thermal conductivity, have indicated an unusual behavior for these properties in the near-critical region. This section is a survey of the literature on the physical and thermodynamic properties for propane.

Density

The PVT data of Sage, Lacey, and co-workers (31,33), Deschner and Brown (12), Beattie, Kay and Kaminsky (4), and the American Petroleum Institute Research Project 44 (3) establish the volumetric behavior of propane in the critical region. These data have been used as the basis for calculated thermodynamic functions for propane recently reported by Canjar, Patel, and Manning (6). Accordingly, their values were used in this investigation.

Figure 1 is a plot of the density-temperature relationship at 700 psia. The functionality at other pressures in the critical region is similar.

Viscosity

The viscosity behavior of propane in the critical region has been accurately determined by Starling (38) and Starling, Eakin and Ellington (37). Their results were obtained using an improved capillary tube viscometer developed at the Institute of Gas Technology. Abnormalities in the viscosity-density isotherms, such as reported for carbon dioxide in the near-critical region, were not observed with propane. The viscosity-temperature behavior at 700 psia is shown in Figure 2.

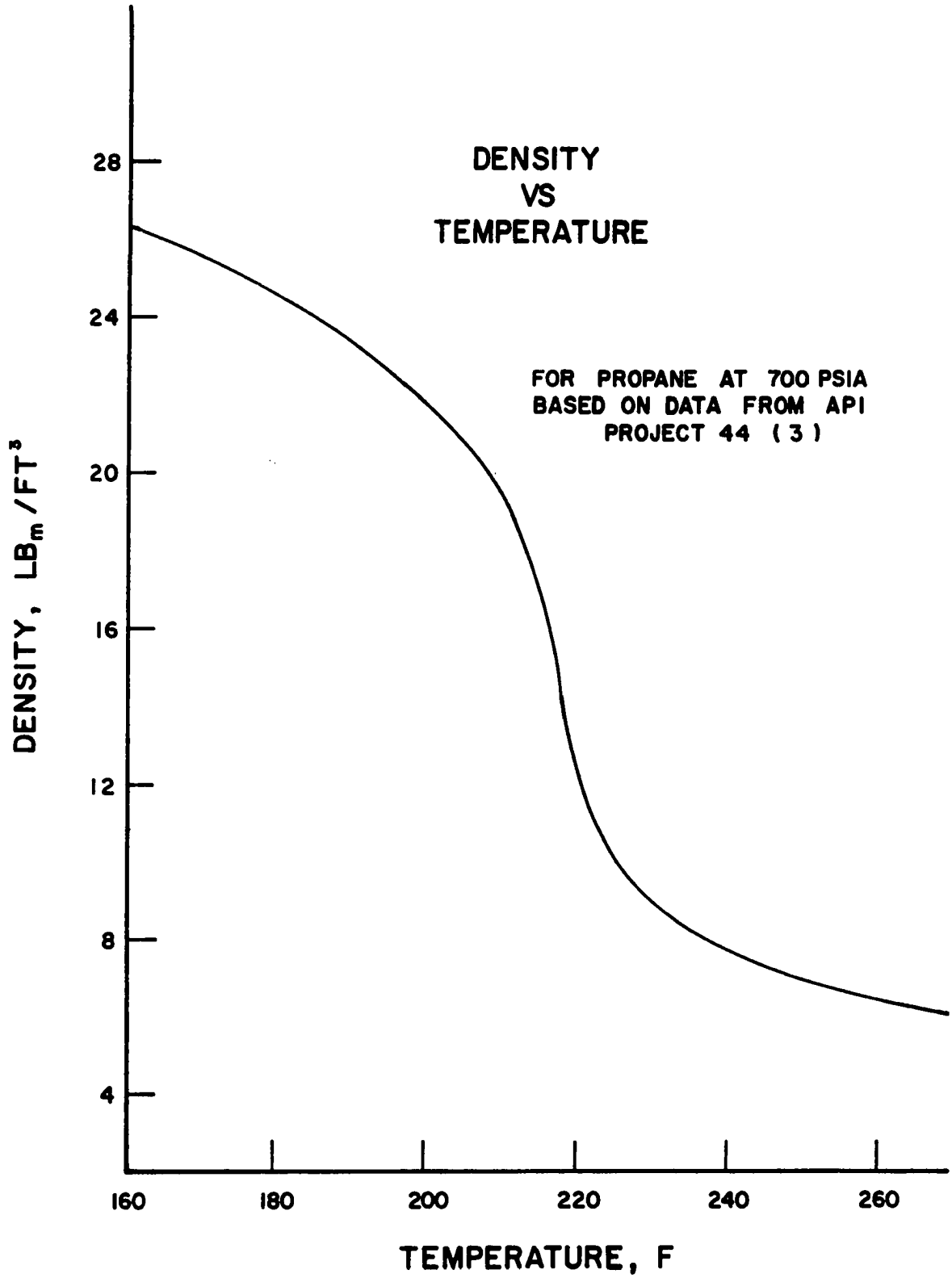

Figure 1. Density-Temperature Behavior at 700 psia

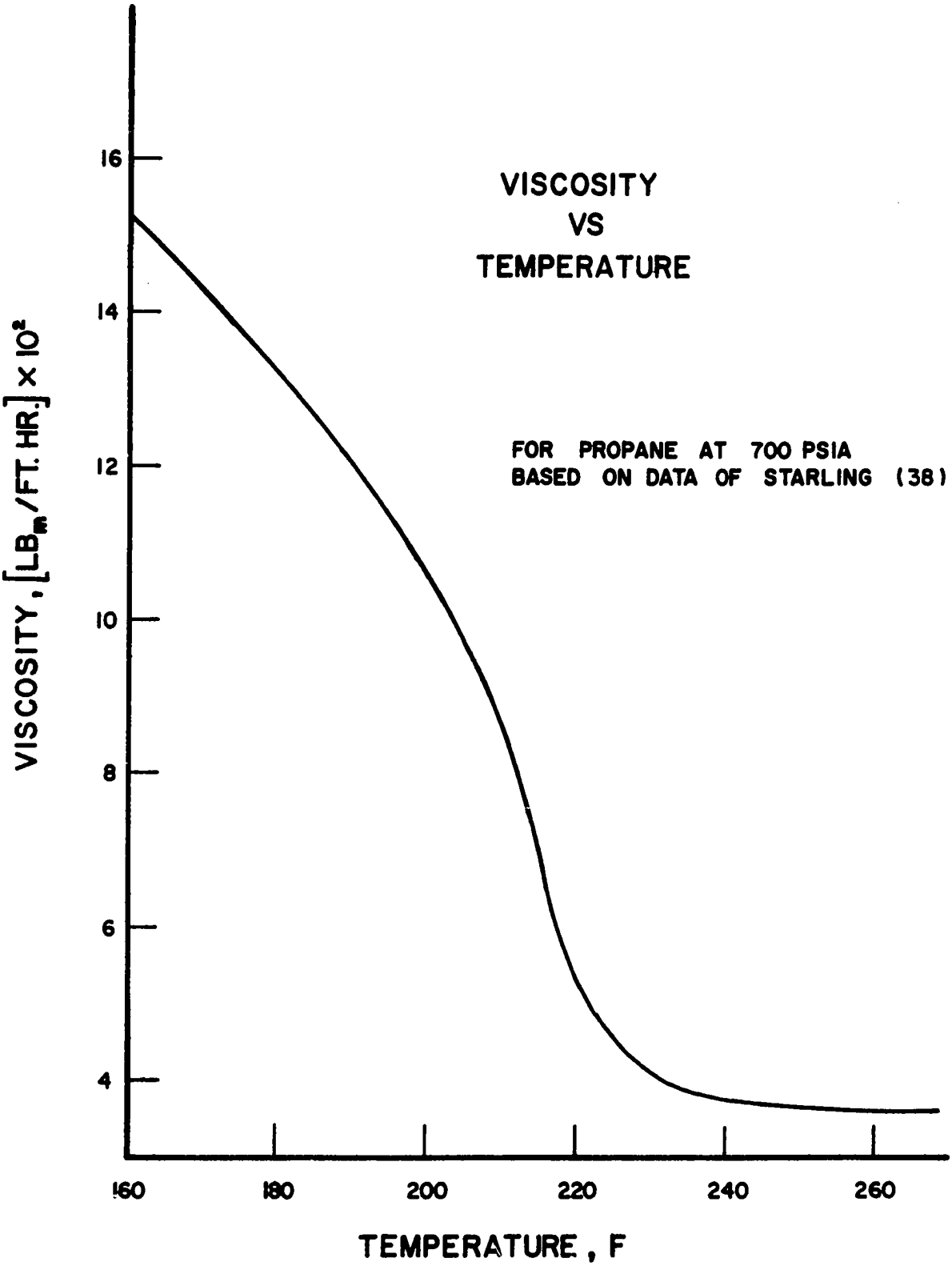

Figure 2. Viscosity-Temperature Behavior at 700 psia

Thermal Conductivity

Leng and Comings (24) have measured the thermal conductivity of propane in both gas and liquid regions at temperatures and pressures above and below the critical point. They observed 'humps' in the thermal conductivity-pressure isotherms at pressures in excess of the saturation pressure. The magnitude of the hump decreased as the temperature increased and was scarcely detectable above 190F.

Their measurements along the isotherm at 222F showed a sharp peak in the neighborhood of 50 atmospheres. This peak was believed to be due to convection since the thermal conductivity decreased appreciably with a decrease in the temperature difference across the fluid layer in the cell. Accordingly, they adjusted their values to smooth out the peak.

Owens and Thodos (26) have reported the thermal conductivity increment, $k - k^0$, where k^0 is the thermal conductivity at one atmosphere pressure, to be a power function of the density in the case of argon. They show a single curve representing the thermal conductivity for both gas and liquid phases. This interesting relation has been attributed to Abas-Zade (1). When plotted in this form, the data of Leng and Comings formed a single curve (within experimental error) as shown in Figure 3. This correlation was used to predict the thermal conductivity for the heat transfer studies.

Enthalpy and Isobaric Heat Capacity

These thermodynamic properties are reviewed jointly

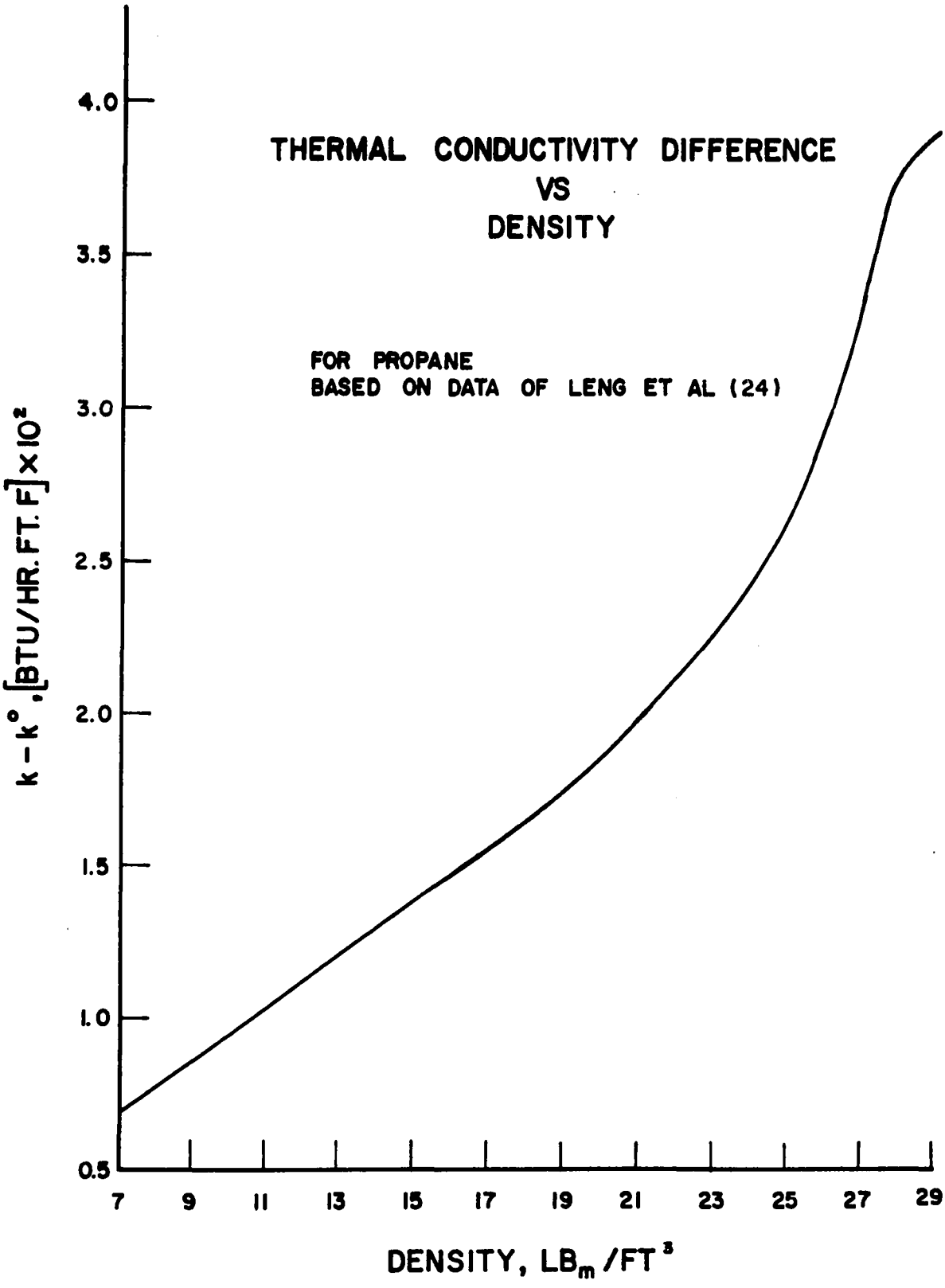

Figure 3. Thermal Conductivity Increment versus Density

because they are related. The isobaric heat capacity, C_p, is the derivative of the specific enthalpy with respect to temperature at constant pressure. Prior to this investigation, caloriometric data were not available for propane in the critical region. The thermodynamic functions reported in the literature have generally been calculated from PVT data and low pressure specific heat values determined caloriometrically or from spectroscopic measurements. The calculated functions require both differentiation and integration of the PVT measurements. This procedure generally gives reliable results for most regions of pressure and temperature. However, it is clear from the volumetric behavior in Figure 1, that the determination of derivatives is inaccurate in the critical region.

The errors inherent in differentiation of PVT data on the critical region are indicated in Figure 4. The data plotted are those of Din (14), Canjar, Patel and Manning (6), and Sage and Lacey (33). The ordinate represents the difference in specific enthalpy between the temperature in question and 180F. Hence, all curves have a value of zero at 180F. This method of plotting was used to eliminate the various reference states employed by the different investigators. The data of Din and Canjar et al. were calculated essentially from the same set of PVT data. The difference in the enthalpies primarily represents differences in smoothing and differentiation of the volumetric data.

Specific enthalpy data are required for the

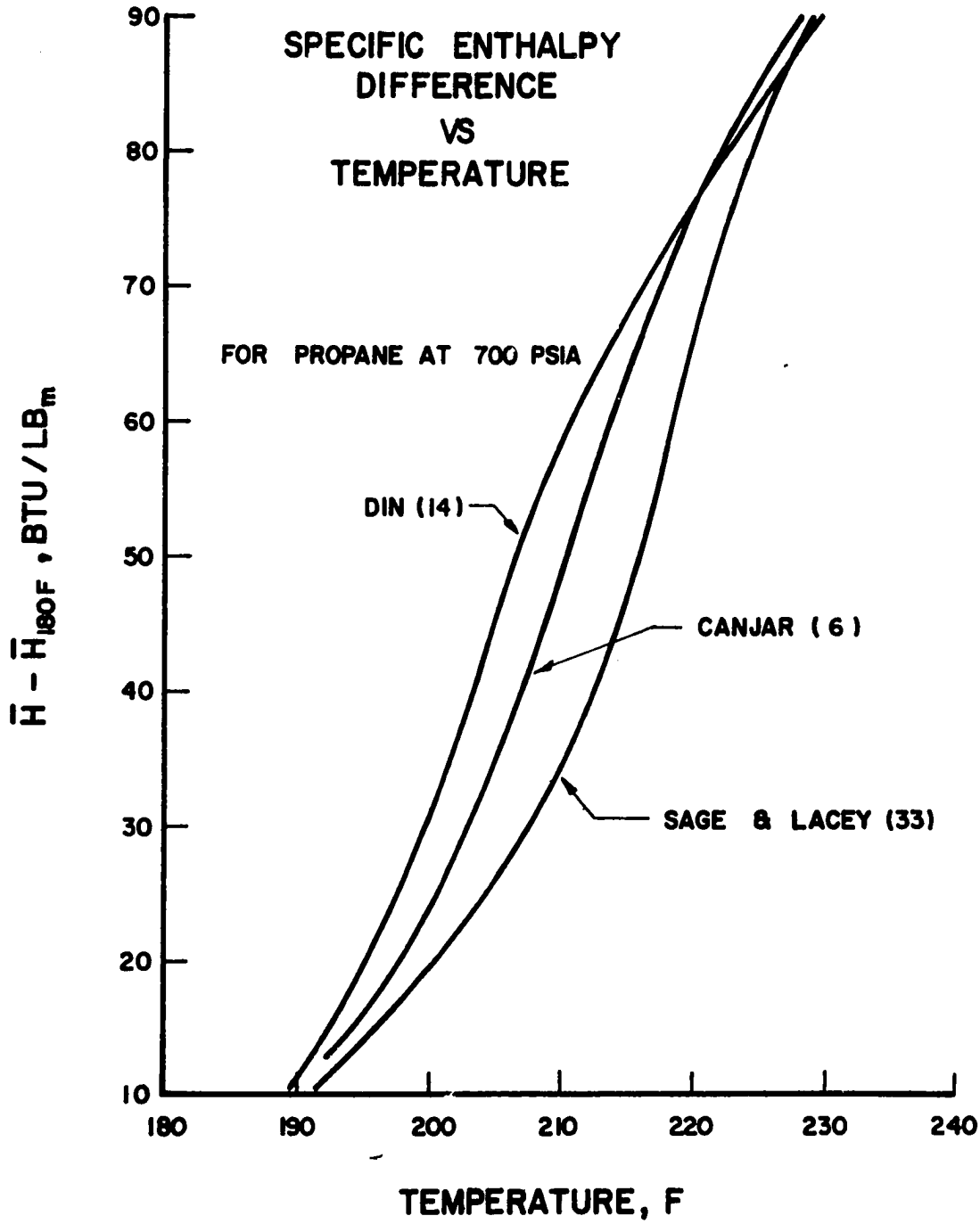

Figure 4. Specific Enthalpy Difference versus Temperature
P = 700 psia

determination of the bulk fluid temperature, which subsequently is used to calculate the heat transfer coefficient defined by Equation (1). The accuracy of these data are included in the overall accuracy of the heat transfer coefficient. For this reason, and because of the differences in the available enthalpy data noted above, the experimental determination of the specific enthalpy was necessary in order to conduct a meaningful study of convective heat transfer in the critical region.

CHAPTER III

THEORY

The present discussion will be concerned with the development of an equation to accurately predict heat transfer coefficients for fluids with large and irregular physical property variations. In order to simplify the development, the discussion will be confined to fully developed turbulent flow through cylindrical tubes. Aside from this limitation, the equation is to be completely general and applicable to any fluid at any thermodynamic state for which the physical properties are known. In the limit, the equation must predict heat transfer coefficients for cases where property variations are small or negligible.

The problem of turbulent heat transfer in cylindrical tubes is usually solved by one of the following methods: (1) the simultaneous solution of the partial differential equations for the conservation of energy and momentum, and (2) integration of the one dimensional transport equations (cf. Deissler (10)). The first approach is lengthy and consequently has been used only with the assumption of constant properties. The second method has been employed by Deissler (10) and Goldmann (16) to solve the case of variable properties

for supercritical water. Both procedures require extensive iterative calculations and as such are limited to application with high speed computers. Because of this limitation, neither of the above methods were considered in the present investigation. It may be that further study with similar techniques might prove fruitful.

Conventional correlations such as Equation (2) have been very successful for predicting heat transfer characteristics in the case of small property variations. Hence the approach used in this study was to examine the effects of property variations on the parameters involved in the Nusselt number,

$$Nu_b = \frac{hD}{k_b} \tag{18}$$

Equation (18) can be rearranged utilizing the definitions for the heat transfer coefficient, Reynolds and Prandtl numbers, and the dimensionless velocity to give

$$Nu_b = \frac{Re_b \, Pr_b \, (\rho_w/\rho_b)}{\left(\frac{(t_w - t_b)\rho_w v_*}{q_w} \right) C_{pb} \, u_b^+} \tag{19}$$

If the first term in the denominator of (19) is multiplied by the specific heat capacity at the wall, C_{pw}, the result is Deissler's dimensionless bulk temperature, t_b^+. However, in order to determine the bulk fluid temperature, the enthalpy flux must be integrated across the tube. The bulk temperature thus corresponds to the bulk specific enthalpy as determined

by

$$H_b = \frac{\int_0^R \bar{H}\rho u r\, dr}{\int_0^R \rho u r\, dr} = \frac{2\int_0^R \bar{H}\rho u r\, dr}{G_b R^2} \tag{20}$$

where:

r = radius variable

R = inside tube radius

$\bar{H}, \rho, u$ = point values of the specific enthalpy, density and fluid velocity as functions of the radius variable

G_b = bulk mass velocity

From the expression for the bulk enthalpy, it is convenient to define a dimensionless enthalpy and mass velocity,

$$H^+ = \frac{(H_w - \bar{H})\ \rho_w\ v_*}{q_w} \tag{21}$$

and

$$G^+ = \frac{\rho\ u}{\rho_w\ v_*} = \frac{G}{\rho_w\ v_*} \tag{22}$$

such that

$$H_b^+ = \frac{(H_w - H_b)\ \rho_w\ v_*}{q_w} = \frac{C_{pm}}{C_{pw}}\, t_b^+ \tag{23}$$

where v_* is the shear velocity defined by Equation (8). The mean integrated specific heat capacity, C_{pm}, is evaluated over the temperature interval between the wall and bulk temperatures.

$$C_{pm} = \frac{\int_{t_b}^{t_w} C_p \, dt}{t_w - t_b} = \frac{H_w - H_b}{t_w - t_b} \tag{24}$$

Equations (19), (22) and (23) may be combined to yield an expression for the Nusselt number in terms of the new dimensionless variables, i.e.,

$$Nu_b = \frac{Re_b \, Pr_b}{(H_b^+ \, G_b^+)} \left(\frac{C_{pm}}{C_{pb}} \right) \tag{25}$$

The dimensionless enthalpy flux in (25) is given by the dimensionless form of Equation (20),

$$H_b^+ \, G_b^+ = \frac{2}{R^+} \int_0^{R^+} H^+ \, G^+ \left(\frac{R^+ - y^+}{R^+} \right) dy^+ \tag{26}$$

where R^+ is the dimensionless tube radius defined by Equation (6).

The integration of the enthalpy flux across the tube requires knowledge of the temperature and velocity profiles. However, this information is not known since the profiles are functions of the system parameters. Deissler (11) and others (5,16) have integrated the radial transport equations to obtain the velocity and temperature distributions. They subsequently integrate these results to yield the bulk temperature and velocity. The purpose of the present development is to investigate the feasibility of replacing these integrations

with an integration at constant properties which is then combined with parameters involving the property variations.

The integration of Equation (26) can be expressed in the form

$$H_b^+ G_b^+ = (H^+ G^+)_{avg} \tag{27}$$

which satisfies the relation

$$(H^+ G^+)_1 < (H^+ G^+)_{avg} < (H^+ G^+)_c \tag{28}$$

where the subscript (1) refers to the edge of the laminar layer and (c) to the tube center. The inequality expressed by (28) is valid regardless of the property variations.

The basic form of the Nusselt number given by Equation (25) yields a better correlating function when expressed in the form,

$$Nu_b = \frac{Re_b\ Pr_b}{(H_b^+ G_b^+)_{t_b}} \left(\frac{C_{pm}}{C_{pb}} \right) \frac{(H_b^+ G_b^+)_{t_b}}{(H^+ G^+)_{avg}} \tag{29}$$

where the subscript t_b refers to constant properties at bulk conditions. If the properties did not vary across the tube radius and they were the same as the bulk values, Equation (29) would reduce to

$$Nu_b = \frac{Re_b\ Pr_b}{(H_b^+ G_b^+)_{t_b}} = Nu_b' \tag{30}$$

The term Nu_b' is frequently referred to as the isothermal bulk

Nusselt number since only in the isothermal case would the properties be constant. Combining Equations (29) and (30),

$$Nu_b = Nu_b' \left(\frac{C_{pm}}{C_{pb}} \right) \frac{(H_b^+ G_b^+)_{t_b}}{(H^+ G^+)_{avg}} \qquad (31)$$

The average or bulk enthalpy flux is principally affected by the heat transfer resistance near the tube wall as indicated by Equation (28). This resistance is characterized by the thermal conductivity, and to a lesser degree, the heat capacity and density in this region (cf. Equation (4)). Since the integrated enthalpy flux evaluated at bulk conditions is only a function of bulk properties, it would seem reasonable that the ratio of the two enthalpy fluxes might be represented by an expression of the form

$$\frac{(H_b^+ G_b^+)_{t_b}}{(H^+ G^+)_{avg}} = \left(\frac{C_{pb}}{C_{pw}} \right)^a \left(\frac{\rho_b}{\rho_w} \right)^b \left(\frac{k_b}{k_w} \right)^c \left(\frac{\mu_b}{\mu_w} \right)^d \qquad (32)$$

where a, b, c, and d are empirical constants. The viscosity ratio has been introduced to account for its effect on the velocity profile.

It has been determined by calculations that when the ratio of the bulk to wall heat capacity is replaced by the bulk to mean value, a better correlation is obtained. This is probably due to the irregular variation of the heat capacity with temperature. Incorporating this idea with Equations (31) and (32),

$$Nu_b = Nu_b' \left(\frac{C_{pm}}{C_{pb}} \right)^{a'} \left(\frac{\rho_b}{\rho_w} \right)^b \left(\frac{k_b}{k_w} \right)^c \left(\frac{\mu_b}{\mu_w} \right)^d \qquad (33)$$

Equation (33) has been used to predict heat transfer coefficients for propane in the supercritical region. The results of these calculations are presented in the Results section.

CHAPTER IV

DESCRIPTION OF EXPERIMENTAL APPARATUS

The experimental apparatus consisted primarily of two elements, a closed heat transfer loop and an external pressure control system. A schematic flow diagram of the apparatus is shown in Figures 5 and 6.

Flow Description

Instrument grade propane, 99.5 mole per cent minimum purity, was circulated through the system by a canned rotor, centrifugal pump. Leaving the pump, the fluid passed through a turbine-type flow meter and on through a needle valve which was used to manually control the flow rate in the loop. The average flow conditions at the meter were determined from a pressure and temperature tap downstream from the meter. The fluid then passed through a shell-and-tube preheater where it was heated by low pressure steam to the desired temperature. The fluid was mixed and its bulk temperature measured with a bare thermocouple in the entrance mixing chamber. The fluid was heated electrically in the Inconel test section. Thermocouples were located on the outside of the tube wall to determine the tube temperature profile. At the outlet of the test section, the fluid was mixed and its bulk temperature again

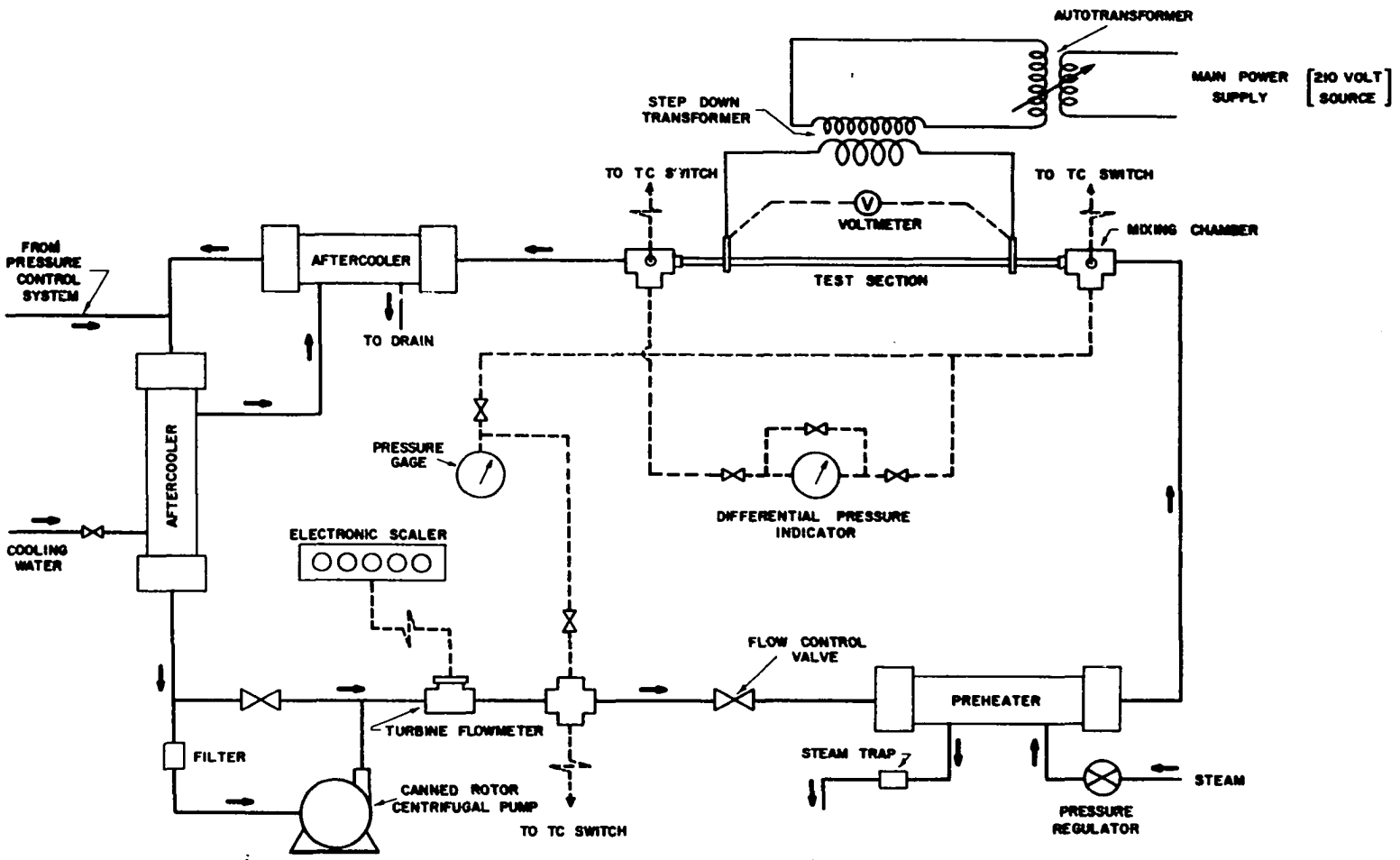

Figure 5. Schematic of Closed Heat Transfer Loop

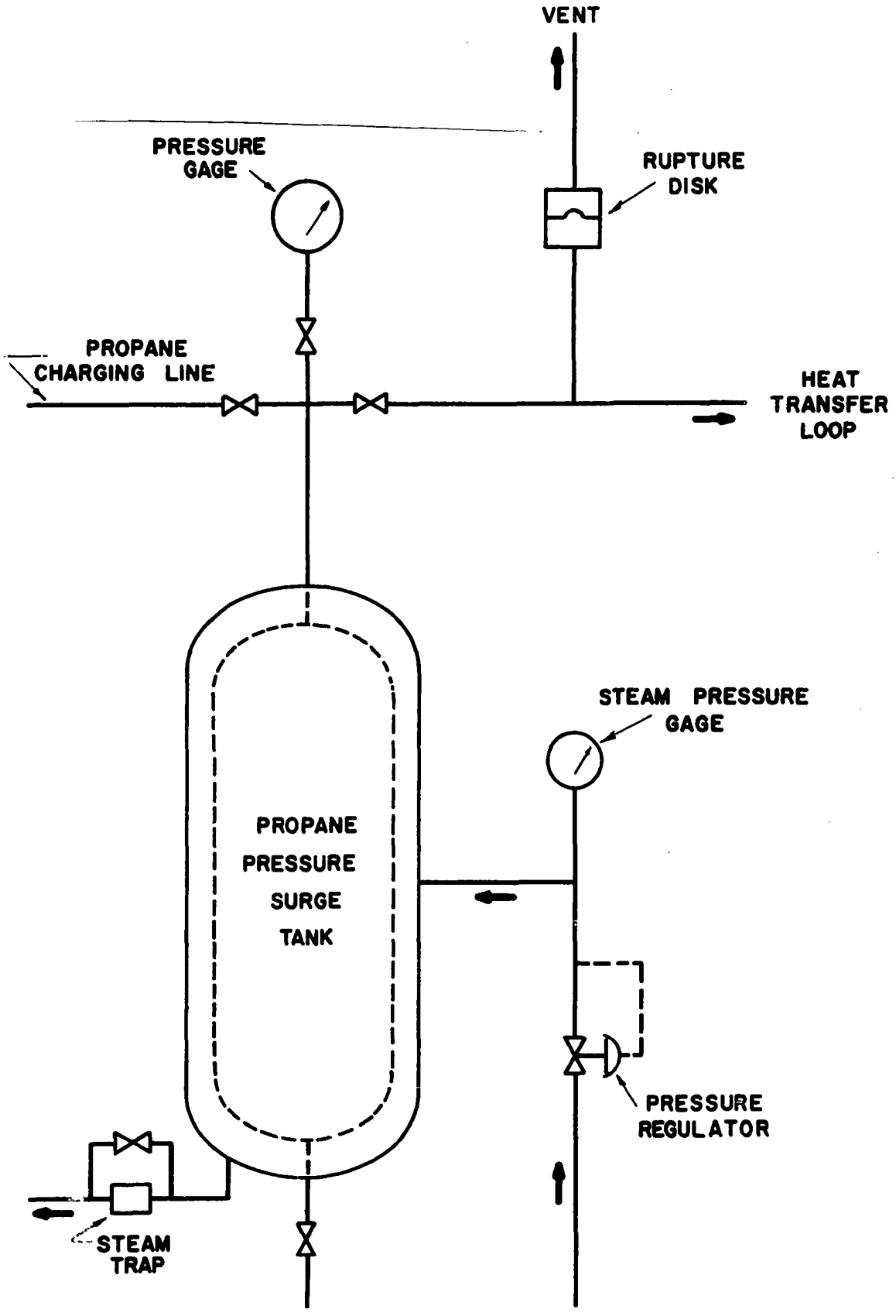

Figure 6. Pressure Control System

measured with a bare thermocouple. Pressure taps were located at each mixing chamber to measure the system pressure and the pressure drop across the test section. The hot fluid from the test section was cooled by tap water in two shell-and-tube aftercoolers and returned to the pump suction, completing the flow cycle.

Test Section

The test section consisted of an Inconel tube, 29 in. long, 0.301 in. inside diameter, with a wall thickness of 0.029 in. Portions of the tube, 4.5 in. at the entrance and 3.5 in. at the exit, served as flow straightners. The remainder of the test section was used as an electrical resistance heater. Details of the test section and the mixing chambers are shown in Figure 7.

Electrical power was supplied to the tube through rubber insulated arc welding cables. The cables were fastened with cap screws to the ends of two copper lugs. The lower ends of the lugs were drilled with 0.3 in. holes. The test section was inserted through the holes and silver soldered to the lugs.

In order to use the test section as a resistance heater, it was necessary to electrically insulate the test section from the rest of the heat transfer loop. The insulation was accomplished at each end of the test section with electrically-insulating pressure fittings as shown in Figure 7. Each fitting consisted of a 1/2 in. male connector

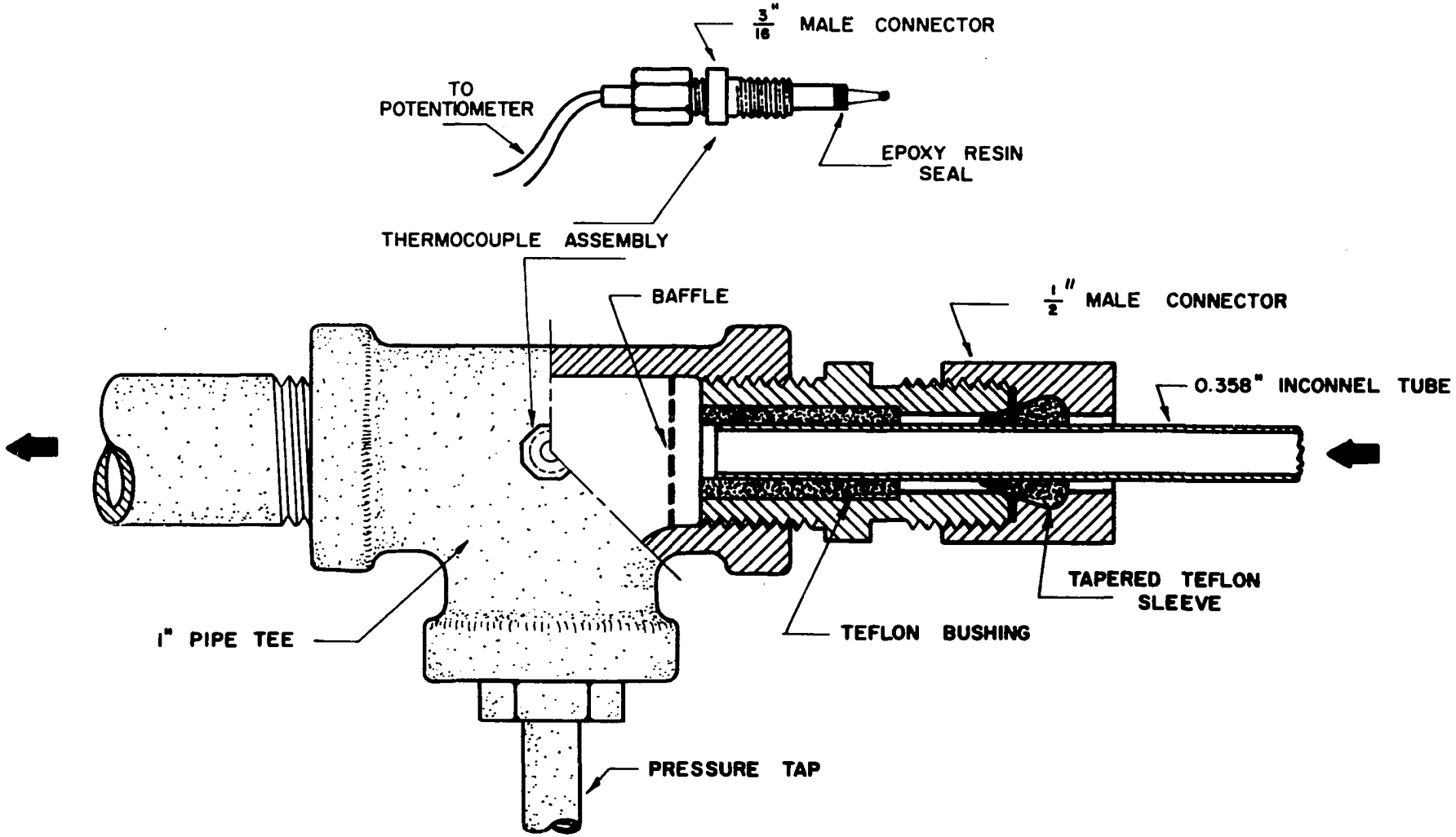

Figure 7. Mixing Chamber Assembly

with a teflon bushing and sleeve. The teflon bushing electrically insulated the test section from the fitting and the rest of the loop. The pressure seal was formed by extrusion of the teflon sleeve with the connector nut. The 1/2 in. connectors were screwed into 1 in. high pressure pipe tees with 1/2 in. bushings.

Thermocouples were silver soldered to the outside of the tube wall at 1 in. intervals. These thermocouples were 24 gage, copper-constantan with fiber glass insulation. The thermocouple leads were wound around the test section several times before passing to the temperature measurement system. This procedure aided in reducing heat conduction losses along the thermocouple lead wires by forming a nearly isothermal length. It also helped to prevent breakage at the thermocouple junction on the tube wall during the movement of the test section.

The mixing chambers were 1 in. high pressure pipe tees. Sufficient mixing of the fluid occurred in the piping prior to the entrance mixing chamber so that no difficulty was encountered in the determination of the entrance bulk fluid temperature. The expansion of the fluid from the test section into the exit mixing chamber, however, did not create sufficient turbulence to insure a uniform fluid temperature. This problem was eliminated by welding a baffle inside the mixing tee. The baffle was constructed from 1/8 in. angle iron with 16 - 1/8 in. holes.

The fluid thermocouple assemblies were screwed into

the sides of the mixing chambers. Each assembly consisted of a 3/16 in. male connector (Ermeto type) and 2 in. of 3/16 in. O.D. tubing. The thermocouple wire was sealed in the base of the tubing with epoxy resin. The fluid thermocouples were 24 gage, fiber-glass insulated copper-constantan.

The test section and mixing chambers were insulated with 3/4 in. of asbestos tape and 2 1/2 in. of fiber glass.

Pump

The fluid was circulated through the closed loop with a canned rotor, centrifugal pump, Chempump Model CF-3/4-3/4S. This unit was designed to handle 30 GPM of fluid at a 30 ft. discharge head. The pump was totally enclosed and all parts in contact with the fluid were made of type 316 stainless steel. The unit was water cooled and equipped with a thermal cut out. The major advantage of this type of pump was that the circulating fluid was not contaminated with lubricants.

Electrical Power System and Measurement

Electrical power for the test section was obtained from a 210 volt, single phase, AC source. The source was applied to a Superior Electric, Model F1256, autotransformer (variac) with a power rating of 7.5 KVA. The variable output voltage of the variac was supplied to a Westinghouse 20/10:1 step-down transformer and its output was fed through rubber insulated cables to the test section. The low voltage power system, including auxiliary equipment, had a maximum power rating of 7.5 KVA.

The power input to the test section was determined from voltage and resistance measurements. The voltage across the test section was measured with a Weston Model 904 (8 range) AC voltmeter which had a rated accuracy of 1/2 per cent of full scale deflection. The resistance of the test section was determined indirectly from the average tube wall temperature and a resistance-temperature calibration curve.

Flow Meter

Flow rates in the closed loop were measured with a Waugh Model FL-8SB turbine flow meter. The meter was designed with a flow range of 0.9 to 7.5 GPM and had a maximum pressure drop of 4.5 psi. The frequency of the output signal from the turbine meter was measured with an electronic scaler and a precision electrical timer, accurate to 0.1 seconds. The volumetric flow rate through the meter was proportional to the frequency.

Heat Exchangers

The test section effluent was cooled in two shell-and-tube heat exchangers. One of the exchangers, Ross Model 201-6EF, contained approximately 2 sq. ft. of surface area made up of 3/8 in. x 20 BWG seamless steel tubes in a single pass. The other aftercooler was constructed with 6 - 1/4 in. stainless steel tubes 16 in. long. The propane was circulated through the tube side of the exchangers and was cooled by tap water flowing through the shell side.

The shell-and-tube preheater was constructed with 9 -

1/8 in. Schedule 80 seamless steel pipes 24 in. long. Propane was circulated through the tube side of the exchanger and was heated by low pressure steam. The fluid temperature at the entrance to the test section was regulated by adjusting the steam pressure on the shell side of the exchanger.

Pressure Control System and Measuring Elements

The pressure control system for the heat transfer loop is shown in Figure 6. The primary element of the control system was a jacketed cylinder. The cylinder was fabricated from 8 in. double extra heavy seamless steel pipe and had a volume of approximately 4 gallons. Accurate control of the system pressure was achieved by regulating the condensation pressure of steam in the jacket.

Static pressures in the heat transfer loop were measured by a 1000 psi Heise Bourdon tube pressure gage with 2 psi scale graduations. The pressure drop across the test section was measured on a Barton Model 200 pressure differential indicator with a range of 0-100 in. of water.

Temperature Measurements

The test section and fluid thermocouple leads were connected to three, Leeds and Northrup, 10 position, thermocouple selector switches. The connections and selector switches were housed in an insulated box to reduce thermal EMF's at the copper-constantan-brass junctions. The thermocouple voltages were referenced with a Joseph Kaye and Company reference junction and power supply. The reference junction

was maintained at 32F ± 0.034F.

The output voltage from the selector switches was grounded through a 25 MFD condenser to reduce AC noise in the recording system. The test section thermocouple voltages were suppressed with a Leeds and Northrup precision potentiometer, Model 8662. The resulting EMF was observed on a Bristol Dynamaster, Model 1PH-560, 0-1MV range, recording potentiometer. The EMF determinations for the three fluid thermocouples were made with a Leeds and Northrup precision potentiometer, Model K2, accurate to 0.0002MV.

General

The loop and pressure control system was equipped with a vacuum pump and water aspirator for evacuation before the introduction of propane.

The equipment was designed for a maximum working pressure of 1200 psia. The piping was primarily 1 in. Schedule 80 seamless steel although other sizes were used for the pump and flow meter connections.

The maximum flow rate was limited by the system pressure drop and pump capacity to approximately 5.5 GPM.

CHAPTER V

EXPERIMENTAL PROCEDURE

System Preparation and Data Collection

The pressure control vessel and heat transfer loop were charged with propane according to the following procedure. The system was first evacuated with a water aspirator and then with a vacuum pump. The pressure was checked with a mercury manometer and when complete evacuation was indicated, the valve was closed between the vacuum pump and the loop. Propane vapor was bled into the loop through the pressure control vessel until the pressure was approximately 30 psig. The propane was vented to the atmosphere and the system was evacuated using the vacuum pump. The same procedure of pressurizing, venting, and evacuation was repeated. After the second purging, the pressure control vessel was charged with approximately 12 lbm of liquid propane. The system was then ready for operation.

The data for each run were collected after the apparatus was at steady state conditions. This was determined by monitoring the inlet and exit mixing chamber thermocouples on the temperature recorder at approximately 10 minute intervals. If the recorded temperature change was no greater than 0.2F

over a 30 minute span, the system was assumed to be at steady state. As a further check, the fluid temperatures were measured at the beginning and end of the period required to collect the data (approximately 15 minutes). If the change was greater than 0.1F, the system was assumed not to be at steady state.

Heat Transfer Coefficient

The irregular and rapid variations in physical and thermodynamic properties in the near critical region make it impossible to maintain a constant heat transfer coefficient along a finite length of tube. Hence, measurements taken over a section of tube would lead to an average value of h which would have little significance. It was therefore necessary to determine a local or point heat transfer coefficient defined by the expression,

$$h = \frac{q_w}{t_w - t_b} \qquad (1)$$

where q_w is the local wall heat flux and t_w and t_b are the inside wall and bulk fluid temperatures respectively.

Wall Heat Flux

Point values of the heat transfer coefficient were determined for propane flowing through an electrically heated Inconel tube. Inconel was selected for this investigation because it has a tensile strength, comparable to most stainless steels, and a very low temperature coefficient of

electrical resistivity. The latter value is reported as 7×10^{-5} F^{-1} in the range 68-930F(2). Therefore, the electrical power dissipation was essentially constant along the tube wall, even though the wall temperature varied because of changes in the fluid temperature and the heat transfer coefficient.

The position-independent value of the heat flux, q_w, was determined from measurements of the electrical energy dissipated in the test section and the average tube wall temperature. The latter value was used to determine the average heat losses and the tube electrical resistance from a temperature-resistance calibration (see Appendix I for resistance and heat loss calibrations). The heat flux, q_w, was defined as

$$q_w = \frac{\dot{Q}}{2\pi RL} = \frac{\left(\frac{JE^2}{\Omega} - \dot{Q}_\ell \right)}{2\pi RL} \qquad (34)$$

where:

E = voltage drop across test section

Ω = resistance of test section, ohms

R = inside tube radius

L = test section length

$\dot{Q}$ = net rate of heat generation

$\dot{Q}_\ell$ = rate of heat losses

J = conversion factor

Wall Temperature

The wall temperature was measured at the outside of

the tube since it was undesirable to disturb the fluid profile inside the tube. The inside wall temperature was determined from the solution of the differential energy balance for the tube wall. Assuming uniform volumetric heat generation and neglecting axial conduction, the differential energy balance for the tube wall is:

$$\frac{d}{dr}\left(kr\,\frac{dt}{dr}\right) = -\frac{q_w\, r}{R(\xi^2 - 1)} \tag{35}$$

where:

r = tube radius variable

k = thermal conductivity of the tube wall

ξ = ratio of outside tube radius to inside tube radius.

The thermal conductivity of Inconel can be represented by a linear function of temperature over the range employed in this investigation. Assuming the outside of the tube to be perfectly insulated, the boundary conditions at $r = \xi R$ are given by:

$$t = t_s \,, \quad \text{at } r = \xi R \tag{36}$$

$$\frac{dt}{dr} = 0 \,, \quad \text{at } r = \xi R \tag{37}$$

The differential energy balance, equation (35), can be integrated twice, applying the boundary conditions to obtain the temperature distribution across the tube wall. The desired inside wall temperature, t_w, is

$$t_s - t_w = -\frac{q_w R}{k}\left\{\frac{1}{2} - \frac{\xi^2 \ln \xi}{\xi^2 - 1}\right\} \tag{38}$$

where k is to be evaluated at the arithmetic mean of t_s and t_w.

Bulk Fluid Temperature

The bulk fluid temperature, t_b, was determined by means of the macroscopic energy balance. For a steady state process, considering the system boundaries as that defined by two arbitrary planes normal to the direction of flow and the inside tube wall, the balance may be written as:

$$\Delta\left(\overline{H}_b + \frac{v^2}{2g_c} + \frac{g}{g_c} Z\right) = \overline{Q} - \overline{W} \qquad (39)$$

where:

$\overline{H}_b$ = bulk specific enthalpy of the fluid

v = bulk velocity of flowing fluid

Z = elevation above an arbitrary datum level

$\overline{Q}$ = heat transferred per unit mass of flowing fluid

$\overline{W}$ = work transferred per unit mass of flowing fluid

g = acceleration of gravity

g_c = dimensional constant

Δ = linear operator, defined as output-input

The term involving the change in the specific kinetic energy was negligible because the velocities and their changes were small. The test section in the experimental apparatus was oriented horizontally and there was no work for the system as defined. Thus equation (39) reduces to

$$\Delta\overline{H}_b = \overline{Q} \qquad (40)$$

The heat transferred per unit mass of flowing fluid may be expressed in terms of the wall heat flux as:

$$\bar{Q} = \frac{\dot{Q}z}{wL} = \frac{2\pi R q_w z}{w} = \frac{2q_w z}{RG_b} \tag{41}$$

where:

z = distance from point of power application (tube entrance)

w = mass flow rate of fluid

G_b = bulk mass velocity, $w/\pi R^2$

Combining equations (40) and (41) gives the change in the specific enthalpy of the fluid between the tube entrance and a point at a distance z from the tube entrance, i.e.,

$$\bar{H}_{bz} = \bar{H}_{bI} + \frac{2q_w z}{RG_b} \tag{42}$$

where the subscript I refers to the entrance of the test section.

The specific enthalpy of the fluid is a function of pressure and temperature. Since the pressure drop across the test section is small, the pressure distribution may be assumed linear with length (z). The effect of pressure on temperature at constant enthalpy can be calculated from volumetric properties and the isobaric heat capacity by the relation

$$\mu' = \left(\frac{\partial T}{\partial P}\right)_{\bar{H}} = -\frac{\left(\frac{\partial \bar{H}}{\partial P}\right)_T}{C_p} \tag{43}$$

where μ' is the Joule-Thomson coefficient and

$$\left(\frac{\partial \bar{H}}{\partial P}\right)_T = \frac{1}{\rho}\left\{1 + \left(\frac{\partial \ell n\ \rho}{\partial \ell n\ T}\right)_P\right\} \qquad (44)$$

Integrating Equation (43) over a small pressure interval, the integrand is essentially constant and the result may be written as

$$t_{bz} = t'_{bz} + \mu'(P_z - 700) \qquad (45)$$

where t'_{bz} is the temperature corresponding to the bulk specific enthalpy, $\bar{H}_{bz}$, at 700 psia and μ' is the Joule-Thomson coefficient at 700 psia and t'_{bz}. Thus, Equations (42) and (45) can be used to calculate the bulk fluid temperature at any location (z).

Point values of the heat transfer coefficient along the length of the tube were calculated from measurement of the heat input (through dissipation of electrical energy), external wall temperature profile (with thermocouples located on the outside of the tube), flow rate (with a turbine flow meter), bulk temperature and static pressure of the fluid at the tube entrance mixing chamber (with a bare thermocouple and pressure gage), and pressure drop across the test section (with a differential pressure gage).

Thermodynamic Measurements

The apparatus was constructed so that it could be operated as a flow calorimeter to obtain specific enthalpy data. This was accomplished by measuring the bulk temperature

of the fluid at the tube exit. Thus, the specific enthalpy at the exit temperature relative to that at the inlet temperature was determined as a function of the exit temperature. The results of such measurements describe the specific enthalpy behavior of the fluid over the range of temperatures studied. As discussed in the Literature Survey section, such data were not available for propane in the critical region. Values calculated from volumetric data are subject to large errors in this region because of the rapid changes in the properties. Hence, the apparatus was used to measure the specific enthalpy of propane in the following manner. The desired pressure (700 psia) and inlet bulk temperature were held constant and the heat input was varied. The outlet bulk temperature was noted for each value of the heat input. The inlet temperature was chosen between 165 - 170F and readings were taken at various exit temperatures up to that corresponding to a heat flux of approximately 100,000 Btu/hr. sq. ft. It was impossible to cover the entire temperature span by varying the heat flux alone. Thus, a higher inlet temperature was selected and the procedure repeated until the outlet temperature exceeded 250F. The data from these runs are presented in the Results section.

The isobaric specific heat capacity, C_p, was calculated from the enthalpy data from the definition,

$$C_p = \left(\frac{\partial \overline{H}}{\partial T} \right)_p \qquad (46)$$

The calculated results of C_p are also presented in the Results section.

Precision of Data

A flow calorimeter cannot be operated at constant pressure. For the specific enthalpy determinations, the pressure drop across the tube was limited to a maximum of 1.5 psi. The effect of small pressure changes was negligible except near the transposed critical temperature, where the pressure correction could be as high as 1.0 Btu/lbm. This effect was calculated from the integrated form of Equation (44) and the data were adjusted accordingly for all runs.

The enthalpy data were used to check the energy balances in the heat transfer tests. The maximum deviation between the measured electrical energy input and the specific enthalpy change of the fluid between the tube entrance and exit was 2.1 Btu/lbm and the average deviation was 0.3 Btu/lbm. The corresponding average enthalpy change was approximately 23 Btu/lbm.

The precision of the enthalpy data can be estimated by considering the accuracy of the individual measurements required for its determination. The fluid thermocouples, which were located in the inlet and exit mixing chambers, were calibrated to 0.02F against a platinum resistance thermometer using a controlled temperature bath of triethylene glycol. The calibration range was divided into six approximately equal intervals of 40F each. Results of the

calibration are shown in Figure 16.

The electrical energy input was determined from voltage and resistance measurements. The voltmeter was accurate to 0.5% of full scale deflection and was equipped with eight separate ranges so that operation was nearly always above half scale. The tube resistance was determined indirectly from the average tube wall temperature by a resistance-temperature calibration. The calibration was accomplished by circulating fluid adiabatically through the insulated tube and measuring the resistance by the potentiometric method. The calibration resistance measurements were accurate to 0.07%. For a more complete discussion of the calibration procedure and the results, see Appendix I.

The turbine flow meter was calibrated by the manufacturer to 0.3% using water as the calibration fluid. Further calibration with water and the meter in place showed that this level of accuracy could be maintained over the range of the meter by using the calibrated meter constant corresponding to the frequency of the output signal. Because of limitations imposed by the heat exchange capacity of the loop, it was impossible to maintain the same metering temperature and, hence, kinematic conditions at the meter for all runs. From dimensional analysis it can be shown that the volumetric flow rate through the meter is a function of the ratio of the output frequency to the kinematic viscosity. Since propane and water are kinematically different, the meter calibration was checked with propane in a region removed from the critical

state by calculating the meter constant from the overall energy balance using the enthalpy data from Din (14). Results of the calibration are given in Appendix I and are different than those obtained using water as the calibrating fluid. The propane calibration was used to determine the mass flow rate for all runs with an accuracy of 0.6%.

The static pressure in the metering tap and the inlet and exit mixing chambers was observed with a Heise Bourdon tube gauge. The gauge was calibrated by the manufacturer and checked with a dead weight tester. The gauge was found to be accurate within 1.0 psi. The pressure drop across the test section was determined with a Barton differential pressure gauge which was accurate to one inch of fluid head.

The thermodynamic data as well as the heat transfer results depend on the wall temperature. These thermocouples were calibrated in place against the fluid thermocouples by circulating propane adiabatically through the test section. This method of calibration was limited to a maximum temperature of 270F by the steam pressure available in the preheater. At the maximum temperature, the deviations were irregular and as large as 2.8F. These corrections from National Bureau of Standard values are attributed to the silver-soldered connections on the tube wall. The deviations were linear with temperature and, therefore, were extrapolated to higher temperatures to complete the calibration for the range of wall temperatures studied. In the calibration range of 70-270F the thermocouples were accurate to 0.2F.

Tube heat losses were determined by supplying electrical energy to the test section with the system under a vacuum. The axial temperature profiles obtained in these tests were relatively flat in the central portion of the tube, (see Figure 18, Appendix I). This indicated that conduction losses from the ends of the tube are small and would not affect the profile in the center of the tube in the actual heat transfer tests. The electrical power dissipation necessary to maintain the central portion of the tube at various temperature levels was also measured during this test. The results of these runs are shown in Figure 19. A comparison of these values with the measured heat input during actual heat transfer runs at the same wall temperature showed that the heat losses did not exceed 0.5%, except on several runs at a low heat flux of approximately 10,000 Btu/hr. sq. ft.

The maximum error in the specific enthalpy determinations can be obtained from the errors in the individual measurements. Combining Equations (40) and (41), neglecting heat losses, and applying logarithimic differentiation, the error in the specific enthalpy change is given by

$$\frac{\delta(\Delta H_b)}{\Delta H_b} = \left[2\left(\frac{\delta E}{E_{max}}\right)\left(\frac{E_{max}}{E}\right) + \left(\frac{\delta \Omega}{\delta t_w}\right)\left(\frac{\delta t_w}{\Omega}\right) + \frac{\delta w}{w}\right] \quad (47)$$

where E_{max} refers to the full scale voltage and δ the error. Taking an average voltage as two-thirds of E_{max}, Equation (47) yields a maximum error of 2.1% or, correspondingly, 0.4 to

0.7 Btu/lbm in the specific enthalpy change. Thus, the average deviation of 0.3 Btu/lbm for the energy balances for the heat transfer tests was within the limits predicted by the errors in the individual measurements.

Several heat transfer tests were made with propane at low temperatures, 100 - 140F, where the property variations are small. The results of one such test are presented in Figure 8. The experimental points shown are the values of the inside wall temperature computed from the observed outside wall temperatures by Equation (38). The bulk temperature was measured at the tube inlet and exit and the intermediate values were computed from the energy balance, Equation (42). Details of the calculation are described in Appendix III. The heat transfer coefficients were computed from Equation (1). The value of the heat transfer coefficient at the center of the tube is approximately 668 Btu/ hr. sq. ft. F, and its value computed from the Dittus-Boelter equation is 691. The Dittus-Boelter correlation, Equation (2) with a = 0.023, b = 0.8, c = 0.4, has been successful for correlating turbulent heat transfer data where property variations are small and uniform. The difference between the measured and computed heat transfer coefficients is approximately 3% in this case. For six runs at low temperature, the maximum deviation was 13% and the average deviation 7%.

For most of the heat transfer tests the wall temperatures were observed to fluctuate randomly, even at temperatures 100F below the critical. These fluctuations are not

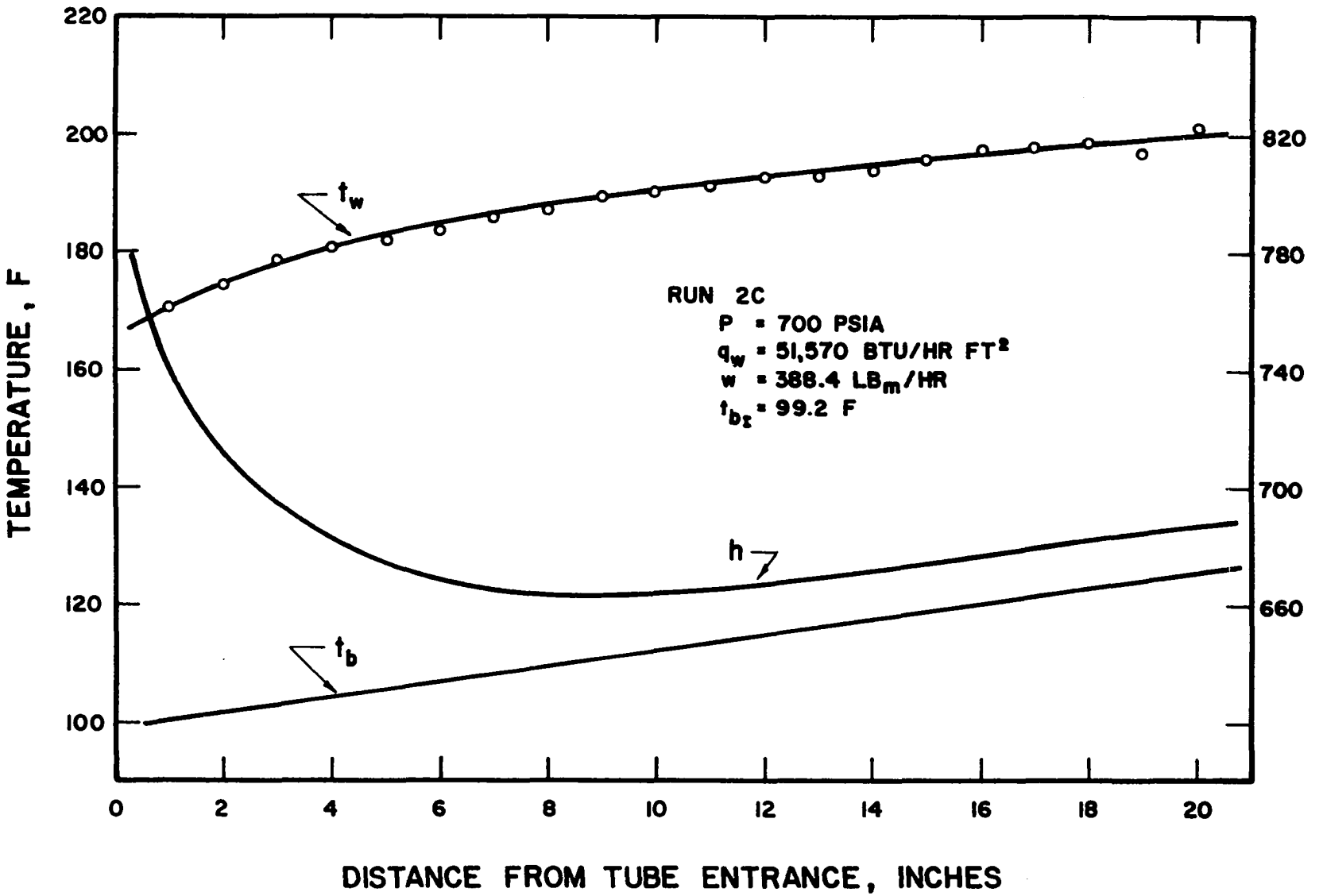

Figure 8. Low Temperature Test Run

understood but appeared to be related to the heat flux, flow rate, and the wall and fluid temperatures. In general the larger the heat flux at given flow rate and fluid temperature, the greater was the fluctuation. It was also observed that certain thermocouples had greater fluctuations under a given set of conditions than others. This characteristic is probably caused by different amounts of silver-solder at the thermocouple junctions. Koppel (22) observed the same fluctuation phenomena in his study of carbon dioxide in the critical region. He postulated that the fluctuations were related to instabilities associated with near-critical fluids or that they were the result of a boiling like process for heat transfer. The fluctuations could also be explained on the basis of the penetration model theory. The maximum amplitude of the fluctuations was 2.5F and the average frequency was 1 cycle per second. The computed inside wall temperatures are based on the mean value of the external wall temperature.

The error in the wall temperatures caused by fluctuations could result in an error of about 3% in the temperature difference, $(t_w - t_b)$, at a temperature of 270F. At higher wall temperatures, the thermocouple errors are likely to be greater since the calibration curves were extrapolated linearly. However, the temperature difference will also be larger and the percent error will thus remain approximately constant. It is also possible that t_b could be in error by as much as 1F due to errors in the enthalpy, fluid temperature measurements, and the flow rate. It therefore seems

unlikely that the error in the temperature difference should exceed 5% except in a few cases of low heat fluxes where $(t_w - t_b)$ was of the order of 3 - 10F. The error in the measurement of q_w was determined in connection with the specific enthalpy change and was found to be less than 2%. On the basis of these considerations it is claimed that the accuracy of the heat transfer coefficient is ±5%, except in the few cases noted previously.

CHAPTER VI

RESULTS

This investigation produced three distinct sets of results: (1) experimental values of the specific enthalpy and isobaric heat capacity for propane at 700 psia, (2) experimental heat transfer coefficients at the same conditions, and (3) correlation of experimental heat transfer data. Accordingly, the presentation is divided into three sections.

Thermodynamic Properties

As discussed in the section titled Experimental Procedure, the results are in the form of specific enthalpy changes as functions of the inlet and exit bulk fluid temperatures. Hence, it was necessary to construct the enthalpy-temperature behavior. The first approach investigated was a graphical solution to the problem. After several trials, the method was discontinued because errors accumulated as the plots were extended to higher temperatures. The second method utilized a least squares computer fit. The basis for acceptability of an equation for the enthalpy was for the average deviation error to be equal to or less than the maximum experimental error of the data (0.4 - 0.7 Btu/lbm).

The enthalpy-temperature behavior of a fluid in the

critical region is characterized by an inflection point at the transposed critical conditions. This unusual behavior in conjunction with the analyticity of the enthalpy function suggested the possibility of an expression of the form,

$$\sigma = f(x) + F(x) \tag{48}$$

where:

$\sigma = \overline{H} - \overline{H}_{t_c'}$

$x = t - t_c'$

t_c' = transposed critical temperature

$f(x)$ = odd function of x

$F(x)$ = even function of x

As a first approximation, the odd and even functions were assumed to be simple power series in x:

$$f(x) = \sum_{i=1}^{10} a_i x^{2i-1} \tag{49}$$

and

$$F(x) = \sum_{i=1}^{5} b_i x^{2i} \tag{50}$$

The coefficients were determined by the "least squares criterion" utilizing the Schmidt orthogonalization algorithm (cf. Pfenning (29)). The average deviation between the data and the resulting equation was found to be greater than the estimated precision of the experimental data. From a graphical analysis, the odd function exhibited parabolic characteristics.

Hence, it appeared reasonable to represent f(x) by a combination of odd and even functions, but retaining the sign properties of the odd function. A similar analysis was employed for the even function, F(x), to give

$$f(x) = \sum_{i=1}^{10} a_i x^i \tag{51}$$

and

$$F(x) = \sum_{i=1}^{5} b_i x^i \tag{52}$$

with the conditions,

$$f(x) = -f(-x) \tag{53}$$

$$F(x) = F(-x) \tag{54}$$

The calculated coefficients of Equations (51) and (52) gave an average deviation of 0.2 Btu/lbm for 75 enthalpy changes used in their determination. This deviation corresponds to an error of approximately 0.9% in the enthalpy change. On this basis, it was assumed that the enthalpy values are accurate to 0.5 Btu/lbm.

Numerous reference states have been employed in presentations and tabulations of specific enthalpies for propane. The American Petroleum Institute (3) has recently published extensive tabulations of thermodynamic properties of propane and other hydrocarbons. To be consistent with these data, it was desirable to report the results on the basis of the following reference state: the specific enthalpy of an ideal gas at

the absolute zero of temperature is numerically zero, i.e.

$$\bar{H}_0^0 = 0 \qquad (55)$$

where $\bar{H}^0$ is the specific enthalpy in the ideal gas state. Conversion of the enthalpy values to this reference state requires a knowledge of the enthalpy change between absolute zero and the lower limit of this investigation, approximately 168F and 700 psia. Since the reference noted above did not contain compressed liquid data at these conditions, the data of Din (14) were used to compute the specific enthalpy relative to the ideal gas state. Din's tabulations are based on the reference state of zero specific enthalpy for the perfect crystalline solid at the absolute zero of temperature. In order to convert Din's values to the ideal gas reference state the specific enthalpy of the perfect crystalline solid must be determined relative to the ideal gas at the absolute zero of temperature. Hence,

$$\bar{H}_0^c - \bar{H}_0^0 = (\bar{H}^0 - \bar{H}_0^0) - (\bar{H}^0 - \bar{H}_0^c) = \text{constant} \qquad (56)$$

where the subscript zero refers to absolute zero and the superscript c, to the crystalline state. Values of the enthalpy of the ideal gas relative to ideal gas state at absolute zero are given in reference (3). The enthalpy of the ideal gas relative to the perfect crystalline solid was determined by extrapolating Din's data to zero pressure. The value obtained for the constant in Equation (56) is

$$\bar{H}_0^c - \bar{H}_0^0 = -265.5 \text{ Btu/lbm} \qquad (57)$$

The specific enthalpy data determined from this investigation are shown in Figure 9 and tabulated in Table I.

The specific heat capacity at constant pressure was calculated from the enthalpy data by means of Equation (46). Substituting the expression for the specific enthalpy, Equation (48), into the definition of the heat capacity yields

$$C_p = \frac{d\sigma}{dx} = f'(x) + F'(x) \qquad (58)$$

The values of the heat capacity thus computed are tabulated in Table I and plotted in Figure 10. At the lower temperature range, 165 - 190F, the calculated heat capacities from Equation (58) exhibited slight oscillations. Accordingly, these values were replaced by the smoothed results obtained from graphical differentiation of the enthalpy data.

The accuracy of heat capacity data obtained from the differentiation of experimental enthalpy changes cannot be ascertained if C_p is a strong function of temperature. In regions where the heat capacity is relatively constant (temperatures less than 190F or greater than 240F) C_p has approximately the same accuracy as the enthalpy data - (1-2%) percent. However, errors may be large near the transposed critical temperature due to uncertainties in the exact location of the transposed critical temperature.

The determination of the transposed critical temperature at 700 psia was more difficult than indicated by Koppel's

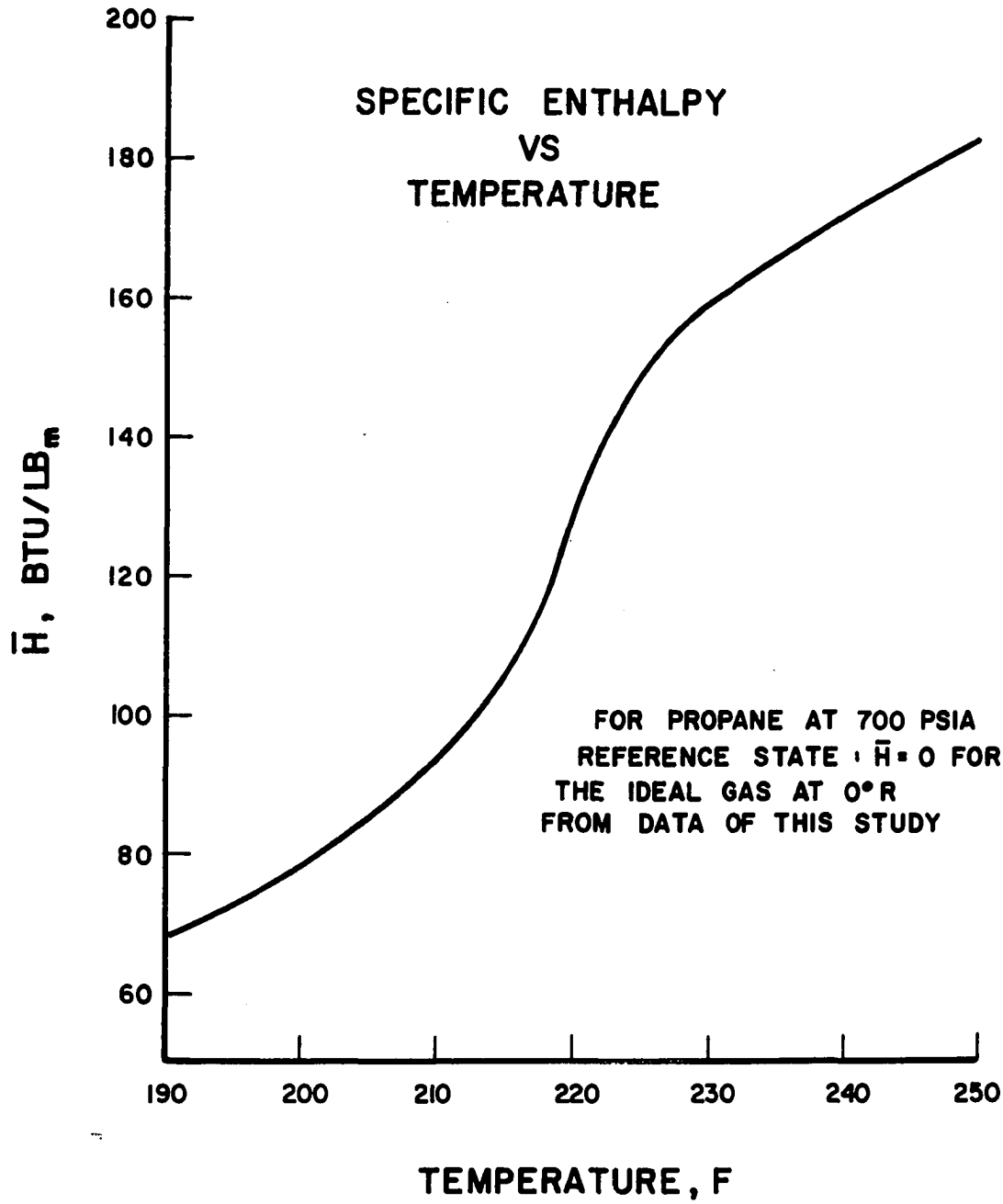

Figure 9. Specific Enthalpy-Temperature Behavior at 700 psia

TABLE I

THERMODYNAMIC PROPERTIES OF PROPANE AT 700 PSIA

REFERENCE STATE: $H_0^0 = 0$ (IDEAL GAS STATE AT ABSOLUTE ZERO)

Temperature, F	$\bar{H}$, Btu/lbm	Cp, Btu/lbmF
168	47.6	0.81
173	51.9	0.86
178	56.3	0.92
183	60.8	0.98
188	65.5	1.03
193	70.6	1.08
198	75.9	1.16
203	82.0	1.35
208	89.7	1.64
209	91.4	1.73
210	93.2	1.83
211	95.1	1.96
212	97.1	2.11
213	99.4	2.36
214	101.9	2.67
215	104.8	3.13
216	108.2	3.74
217	112.3	4.45
218	117.2	5.33
219	123.0	6.60
220	129.2	5.70
221	134.5	4.90
222	138.9	4.05
223	142.7	3.49
224	146.0	3.03
225	148.8	2.63
226	151.2	2.32
227	153.4	2.08
228	155.4	1.89
229	157.2	1.72
230	158.9	1.60
231	160.4	1.49
232	161.9	1.40
233	163.2	1.32
234	164.5	1.25
235	165.7	1.19
240	171.6	1.06
245	177.3	0.99
250	182.7	0.92

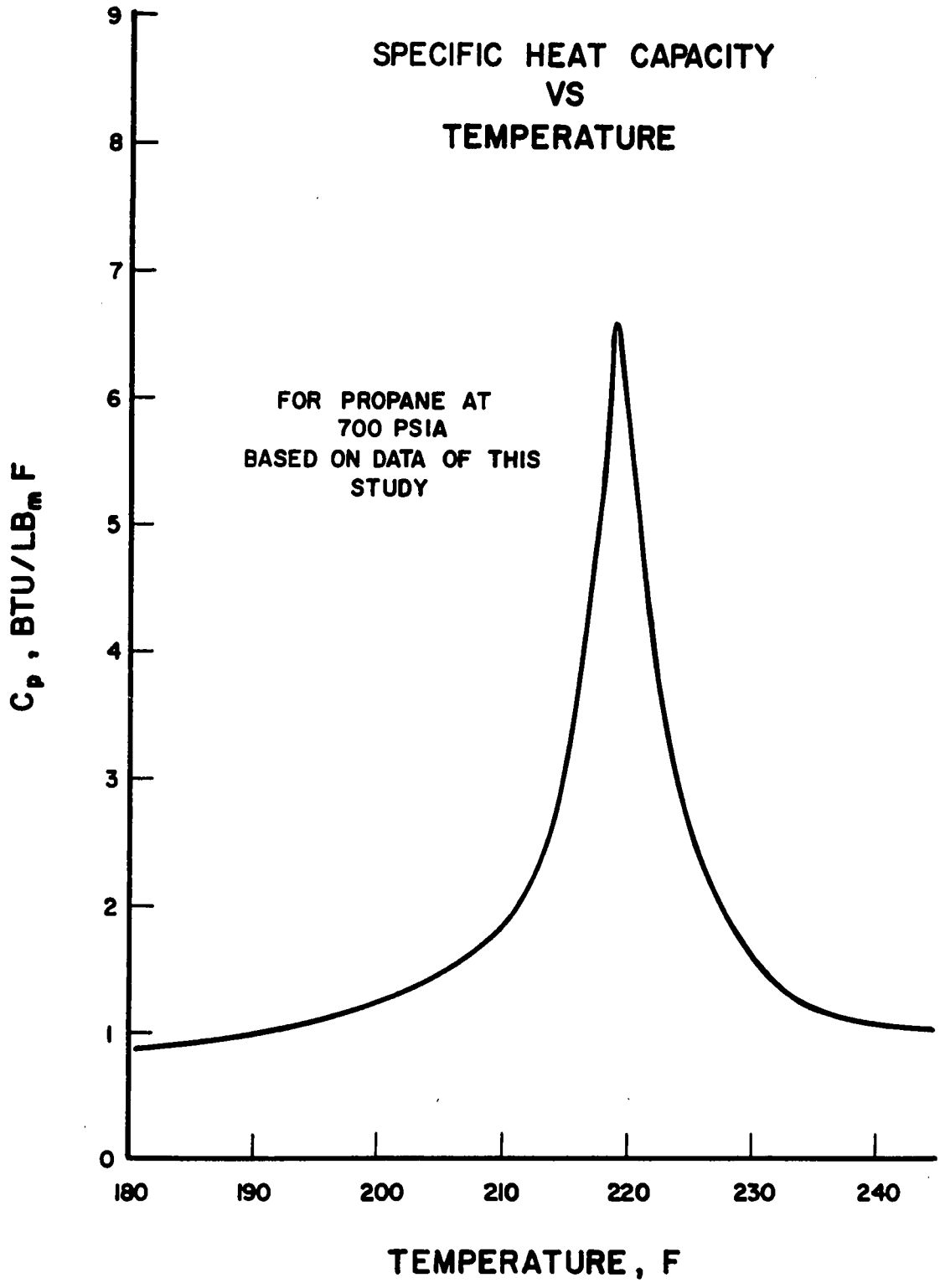

Figure 10. Isobaric Specific Heat Capacity-Temperature Behavior at 700 psia

study of carbon dioxide in the near critical region (22). The point of steepest ascent of the enthalpy-temperature isobar appeared at approximately 219F. The accuracy for the transposed critical temperature is probably no greater than ± 0.3F.

The data presented in Table I serve to define with good accuracy the behavior of the enthalpy and the heat capacity for propane at 700 psia. The results are subject to certain experimental errors but are more accurate than any previously available.

Experimental Heat Transfer Data

The experimental apparatus was used to measure turbulent heat transfer coefficients for propane at 700 psia under the following range of experimental conditions:

Reynolds number:	80,000 to 800,000
Heat transfer rate:	10,000 to 110,000 Btu/hr.sq.ft.
Bulk fluid temperature:	100F to 255F

The critical point of propane occurs at 617.4 psia and 206.3F. The pressure investigated corresponds to a reduced pressure of 1.13 and the temperature range to a reduced temperature interval of 0.84 to 1.07.

The results of a typical experiment, Run 8c, are shown in Figure 11. The wall temperature increases continuously along the length of the tube after a more rapid increase in the entrance region. The local heat transfer coefficient calculated from Equation (1) decreases in the entrance section and becomes relatively constant in the remainder of the tube.

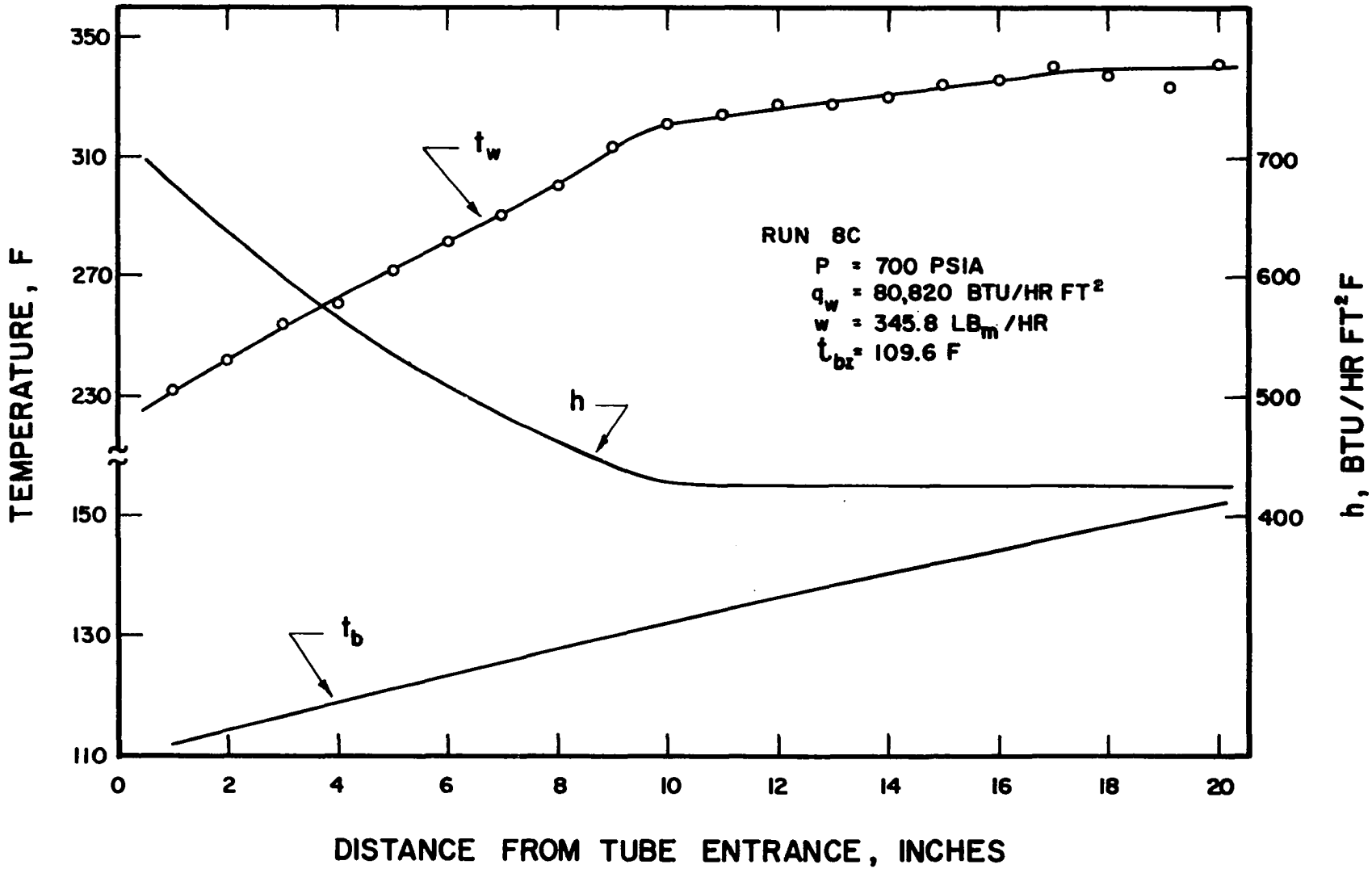

Figure 11. Results of Run Number 8c

The behavior of the heat transfer coefficient after the entrance region will depend on the wall and bulk temperature profiles as indicated by the derivative of Equation (1),

$$\frac{dh}{dz} = \frac{q_w}{(t_w - t_b)^2}\left(\frac{dt_b}{dz}\right)\left(1 - \frac{dt_w}{dt_b}\right) \tag{59}$$

Hence, the heat transfer coefficient will increase, decrease, or remain constant depending on whether the ratio of the slopes of the wall-to-bulk temperature profiles is less than, greater than, or equal to unity. The slopes of the two profiles are primarily related to the specific heat capacities at the wall and bulk fluid temperatures. For a fully developed turbulent mass velocity profile and a constant heat flux boundary condition, it can be shown that

$$\frac{d\bar{H}_w}{dz} - \frac{d\bar{H}_b}{dz} = \varphi \tag{60}$$

where φ is a complicated function of the properties near the tube wall and which, in general, satisfies the condition,

$$\varphi << \frac{d\bar{H}_b}{dz} \tag{61}$$

Combining Equations (60), (61), and the definition for the specific heat capacity

$$\frac{dt_w}{dt_b} \simeq \frac{C_{pb}}{C_{pw}} \tag{62}$$

If the specific heat capacity is a monotonic increasing function of temperature such as for supercritical fluids below

their transposed critical temperature, $C_{pw} > C_{pb}$, and in general the heat transfer coefficient increases with length after the entrance region (cf. Figure 12). Similarly, if C_p is monotonic decreasing, anologous to fluids slightly above the transposed critical temperature, $C_{pb} > C_{pw}$, and h decreases with tube length (Figure 13). When the ratio of the wall to bulk heat capacities is approximately unity, h is essentially invariant with length (Figure 11).

The effect of the wall heat flux on the heat transfer coefficient is indicated in Table II. In the first case listed, the Reynolds numbers based on bulk properties ranged from 313,000 to 317,000 while the bulk temperature varied slightly from 217.5F, approximately one degree below the transposed critical temperature. As the heat flux is increased, the wall temperature increases rapidly resulting in a decrease in the thermal conductivity and heat capacity at the wall. Consequently the resistance to heat transfer in the sublayer adjacent to the wall becomes large and the heat transfer coefficient decreases. The effect of increasing the heat flux is to increase the temperature gradient in the sublayer and decrease the density. The result should be a higher velocity gradient in the sublayer and correspondingly a lower gradient in the bulk core of the fluid. Wood and Smith (39) have measured radial velocity and temperature distributions for carbon dioxide in the critical region. They observed under similar conditions a flattening of the velocity and temperature profiles as the heat flux was increased. These

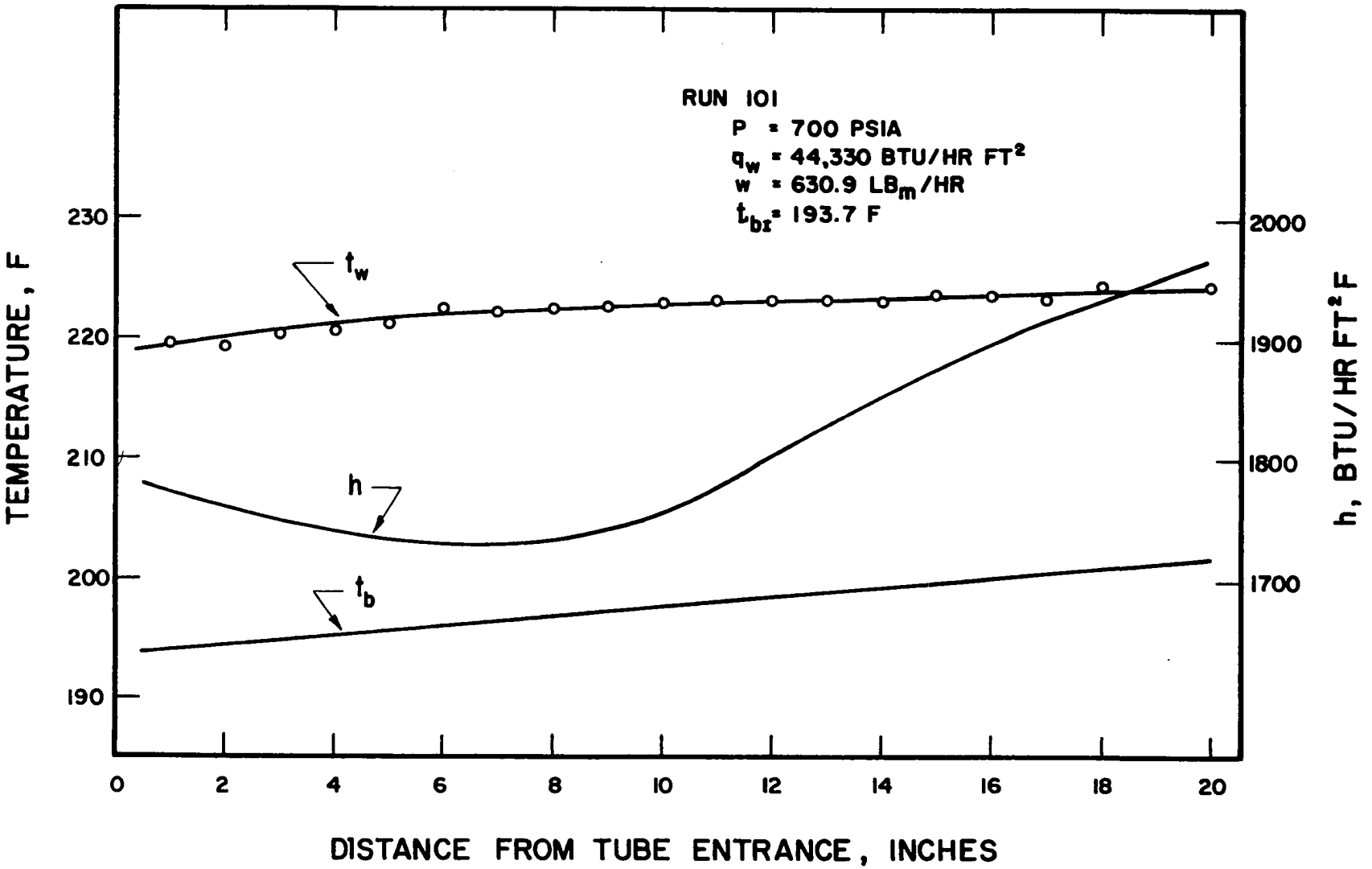

Figure 12. Results of Run Number 101

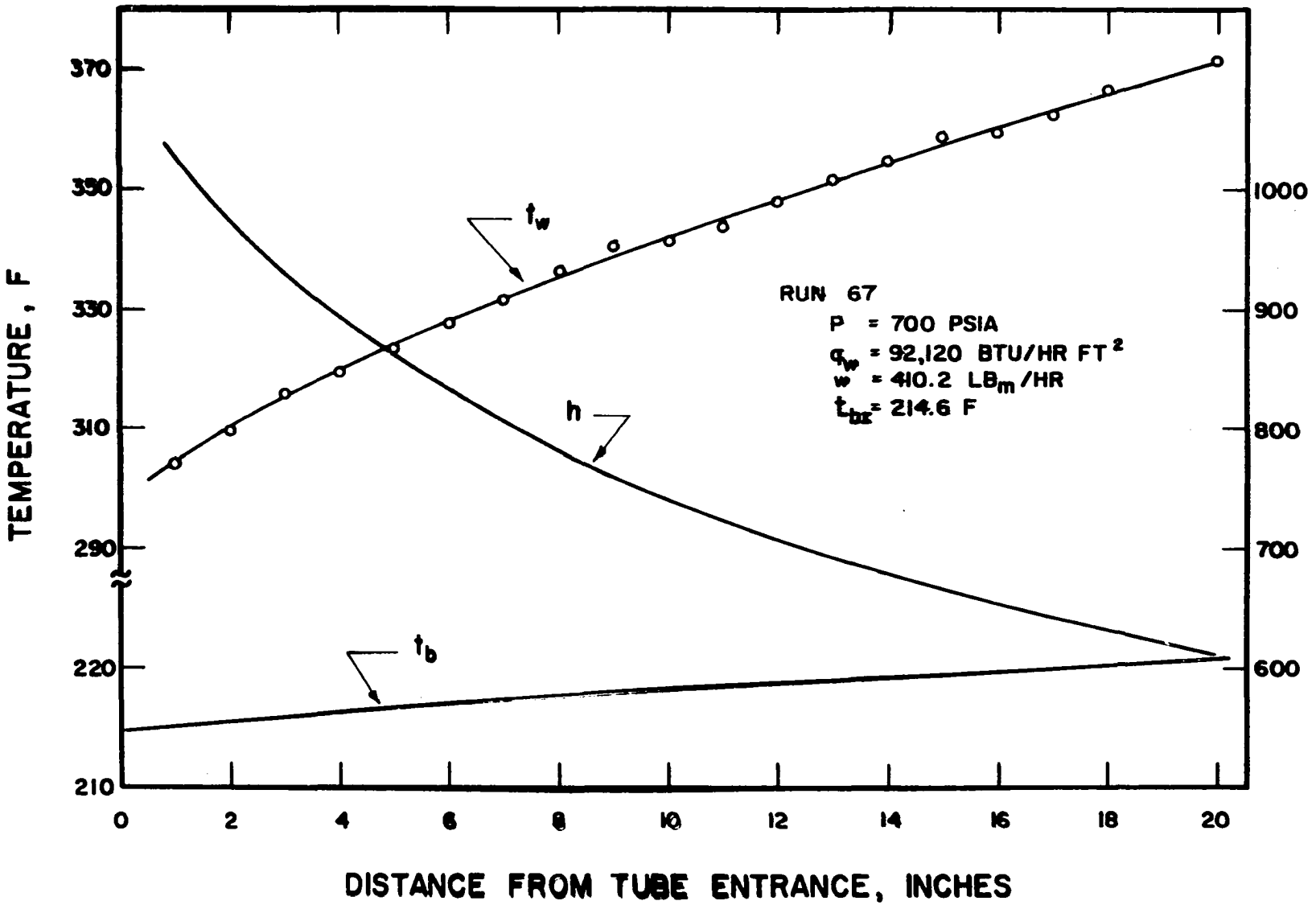

Figure 13. Results of Run Number 67

TABLE II

EFFECT OF HEAT FLUX ON THE HEAT TRANSFER COEFFICIENT

Pressure = 700 psia

Run No.	Heat Flux, q_w Btu/hr.ft^2.	t_b, F	t_w, F	h, Btu/hr.ft^2.F
Bulk Reynolds Number = 3.15 x 10^5				
126	9,700	217.5	221.7	2291
115	21,000	217.5	228.5	1901
112	44,960	217.6	259.4	1075
110	97,700	218.7	392.1	563
Bulk Reynolds Number = 1.82 x 10^5				
3	29,600	175.5	202.5	1095
4	39,300	175.9	211.8	1091
5	53,600	175.9	223.9	1129
15	73,100	176.0	247.3	1024
16	95,600	176.6	290.0	842

observations are in accord with the above reasoning.

For the second case listed in Table II, the bulk Reynolds number was approximately constant at 182,000 and the bulk fluid temperature was well below the transposed critical. As the heat flux is increased, the heat transfer coefficient remains approximately constant until the wall approaches the transposed critical temperature. The heat transfer coefficient then increases slightly due to the large increase in the specific heat capacity in the sublayer. However, as the heat flux is further increased, the result is a decrease in h as noted in the previous case.

Wood and Smith (39) postulated that the effect of heat flux on the heat transfer coefficient could be approximated by an expression of the form

$$h \sim \frac{1}{t_w - t_c'}$$

The data in Table II are in agreement with this model, h is a maximum at a wall temperature near the transposed critical, t_c'.

The rapid decrease in the heat transfer coefficient as the wall temperature exceeds the transposed critical is emphasized in Figures 12 and 14. In Run 101, the wall temperature is slightly above t_c' and remains essentially constant along the entire length of the tube. After entrance effects, the heat transfer coefficient increases rapidly with tube length. In Figure 14, Run 12c, the wall temperature similarly

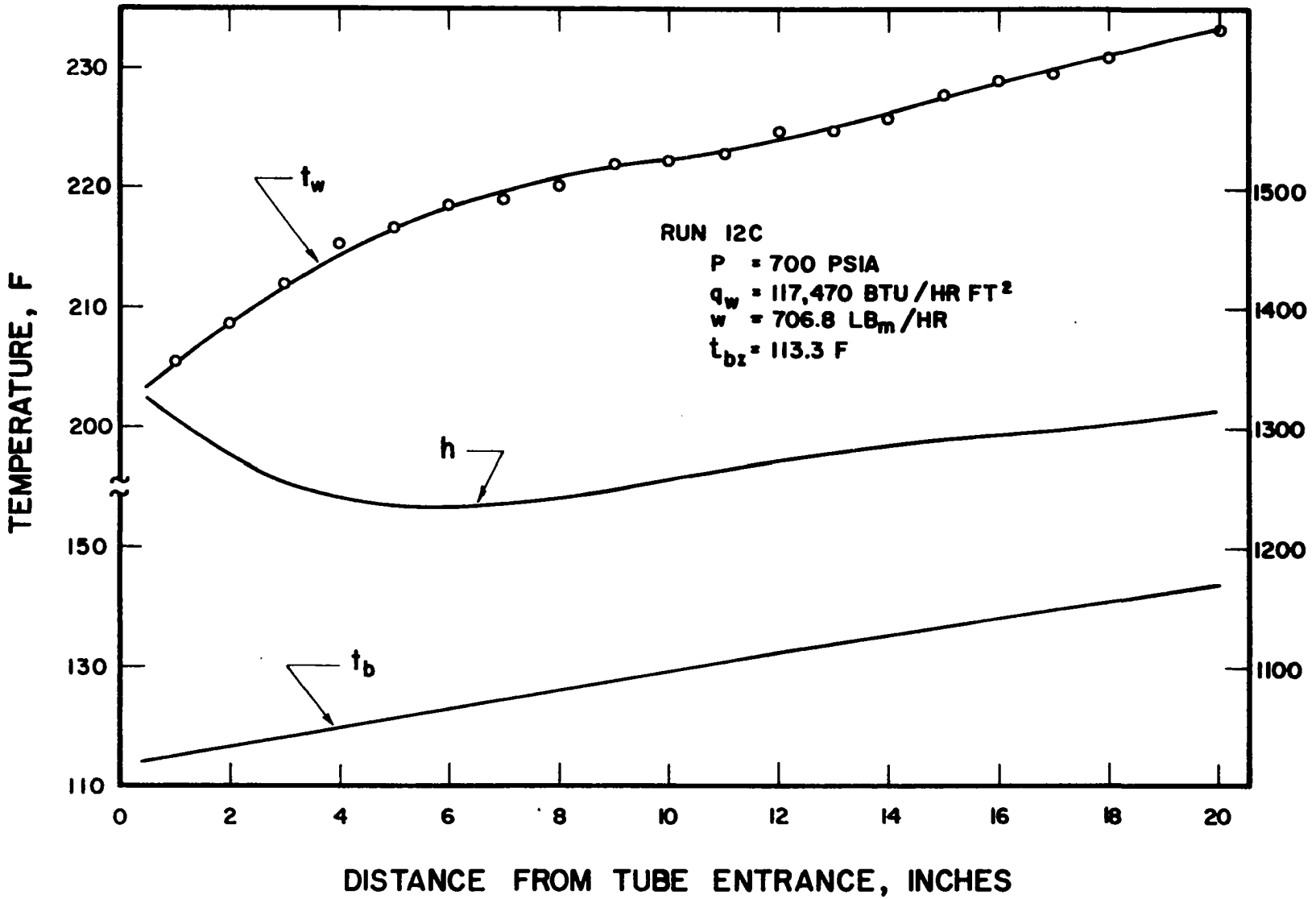

Figure 14. Results of Run Number 12c

is at t_c'. As the wall temperature increases its profile appears relatively flat until it reaches 224F. In this interval h increases with length, but not so greatly as in Run 101. At 224F the slope of the wall temperature profile markedly increases, resulting in a decrease in the slope of h with length. The reason for this apparent sudden change is not understood but is probably caused by the rapid decrease in the specific heat capacity and thermal conductivity at this temperature.

Wood and Smith (39) have concluded from their experimental observations on carbon dioxide in the near-critical region that the relative maximum in the heat transfer coefficient is "properly associated" with the bulk fluid temperature and not the wall temperature. However, their arguments to support this conjecture are inconclusive. They observed relative maximums in both h versus t_b and h versus t_w at constant heat flux and Reynolds number. In a plot of the former type (h vs. t_b), the relative maximum occurs at a temperature below the transposed critical temperature while a plot of the latter yields a relative maximum at a temperature greater than t_c'. For the limiting case as the heat flux approaches zero - equivalent to heat transfer at constant properties - the two curves must coincide and an absolute maximum will occur at the transposed critical temperature. Hence,

$$\lim_{t_w \to t_b} h = h_t' \qquad (63)$$

and

$$h'_t < h'_{t_c} \quad ; \quad t \neq t_c \tag{64}$$

where h'_t is the heat transfer coefficient at constant fluid properties evaluated at temperature, t. The data of this investigation do not include enough values for one heat flux and one flow rate to form a plot of this nature. However, an inspection of Table VI reveals that the relative maximum in the heat transfer coefficient becomes smaller, is less pronounced, and is displaced further from the transposed critical temperature as the heat flux is increased.

The experimental heat transfer data obtained in this investigation are tabulated in Table VI, Appendix II. For each run, the following data are recorded: (1) inside wall temperature profile, (2) bulk fluid temperature at the tube inlet and exit, (3) pressure at the tube entrance, (4) pressure drop across the test section, (5) wall heat flux, (6) mass flow rate, and (7) the value of the heat transfer coefficient at a point 11 inches from the tube entrance. The heat transfer coefficients were computed from Equation (1). A sample calculation for the reduction of test data is given in Appendix III.

Correlation of Heat Transfer Data

A comparison of the experimental data with the correlation of Petukhov et al., Equation (14), is given in Table III. It is evident from these results that his correlation predicts consistently high coefficients (20 - 80%). However, as the

TABLE III

COMPARISON OF EXPERIMENTAL DATA WITH PETUKHOV'S CORRELATION (14)

Pressure = 700 psia

h evaluated at z = 11"

Run No.	h(experimental) Btu/hr.ft.^{2}F	h(calculated) Btu/hr.ft.^{2}F	Heat flux $q_w \times 10^{-3}$ Btu/hr.ft.^{2}
1c	671	824	65.1
2c	666	714	51.6
3c	926	1056	84.8
4c	918	963	60.3
5c	1131	1242	97.2
6c	1382	1443	112.1
7c	601	705	55.6
8c	426	789	80.8
9c	810	961	76.6
10c	900	1094	85.8
2	1057	990	20.5
3	1041	1011	29.6
4	1076	1115	39.3
5	1129	1334	53.6
6	1136	1334	67.6
13	1063	1143	39.9
14	1123	1340	58.5
15	999	1287	73.1
16	854	1218	95.6
11c	1033	1170	93.1
12c	1274	1476	117.5
13c	1706	1686	127.8
14c	1040	1266	105.5
49	1169	1480	82.8
53	1060	1416	81.0
54	1123	1432	81.4
56	983	1291	82.1
57	1027	1346	81.8
58	1033	1402	82.3
62	790	1341	98.9
64	883	1451	81.5
66	828	1476	79.6
75	914	1323	89.1
76	811	1525	87.6
79	719	1250	89.2

TABLE III - continued

Run No.	h(experimental) Btu/hr.ft.^{2}F	h(calculated) Btu/hr.ft.^{2}F	Heat flux $q_w \times 10^{-3}$ Btu/hr.ft.^{2}
81	955	1385	83.3
82	910	1365	83.6
84	999	1458	82.4
86	900	1519	84.0
87	836	1542	84.3
88	785	1488	92.1
89	872	1035	80.8
91	844	1076	97.1
94	1053	1300	75.3
96	951	1306	87.6
99	1132	1486	70.3
101	1776	1932	44.3
103	2363	2666	43.1
104	3490	3724	44.8
105	3619	3794	44.1
107	726	1405	92.1
109	452	1205	107.7
111	4048	4053	43.7
115	1953	1944	21.0
117	2896	2933	21.1
118	3446	3187	20.8
121	4951	4498	21.6
122	4499	4511	20.6
127	2108	2135	9.8

heat flux is reduced, the correlation becomes more accurate and in the limit, the form for the isothermal Nusselt number accurately predicts the heat transfer coefficient, h_t'. The differences between the experimental and the calculated heat transfer coefficients are believed due primarily to the following factors: (1) the preponderance of correlating data at reduced pressures greater than 1.15 and with relatively small wall-to-bulk fluid temperature differences, and (2) an incorrect form of the equation to account for radial variations of the fluid physical properties. The latter reason is more fundamental.

In order to apply the correlation proposed in the Theory section, it was necessary to determine an expression for the isothermal Nusselt number and the unknown constant exponents. Petukhov's correlation gives excellent agreement between experimental and calculated heat transfer coefficients for small wall-to-bulk fluid temperature differences. Hence, Equation (16) was used to predict the heat transfer coefficient at constant properties evaluated at bulk conditions;

$$h'_{t_b} = \frac{k_b Nu'_b}{D} = \frac{k_b}{D} \left\{ \frac{Re_b \, Pr_b \left(\frac{f_b}{2} \right)}{12.7 \left(\frac{f_b}{2} \right)^{1/2} \left(Pr_b^{2/3} - 1 \right) + 1.07} \right\} \qquad (65)$$

The proposed correlation, Equation (33), can be written as

$$h = h'_{t_b} \left(\frac{C_{pm}}{C_{pb}} \right)^a \left(\frac{\rho_b}{\rho_w} \right)^b \left(\frac{k_b}{k_w} \right)^c \left(\frac{\mu_b}{\mu_w} \right)^d \qquad (66)$$

which becomes linear in the logarithimic form. The exponents, (a, b, c, d), were determined by the least squares criterion as discussed previously. Local heat transfer coefficients for 40 runs at positions corresponding to 11 and 12 inches from the tube entrance were utilized in their determination. The computed values yield the following expression:

$$h = h'_{t_b} \left(\frac{C_{pm}}{C_{pb}} \right)^{0.54} \left(\frac{\rho_b}{\rho_w} \right)^{0.27} \left(\frac{k_b}{k_w} \right)^{0.20} \left(\frac{\mu_b}{\mu_w} \right)^{0.02} \qquad (67)$$

Equation (67) was used to compute heat transfer coefficients for each run at five locations: 9 through 13 inches at 1 inch intervals. For each run, the average ratio of h calculated to h experimental for these locations is shown in Figure 15 as a function of the bulk fluid temperature. A majority of the runs (85%) have discrepancies within ±10% and only 3% deviate more than 20% from the experimental values. Near the transposed critical temperature, the region of largest physical property variations, the correlation yields relatively larger deviations. However, these discrepancies are within the limits of error for the combined precision of the experimental determination and the physical property evaluations.

Equation (67) represents an extension of the correlation of Petukhov and associates. They excluded the effect of density variations and this does not seem to be warranted from either a theoretical or empirical basis. Semitheoretical expressions for the heat flux and shear stress contain density effects, cf., Equations (3) and (4). Therefore, this effect

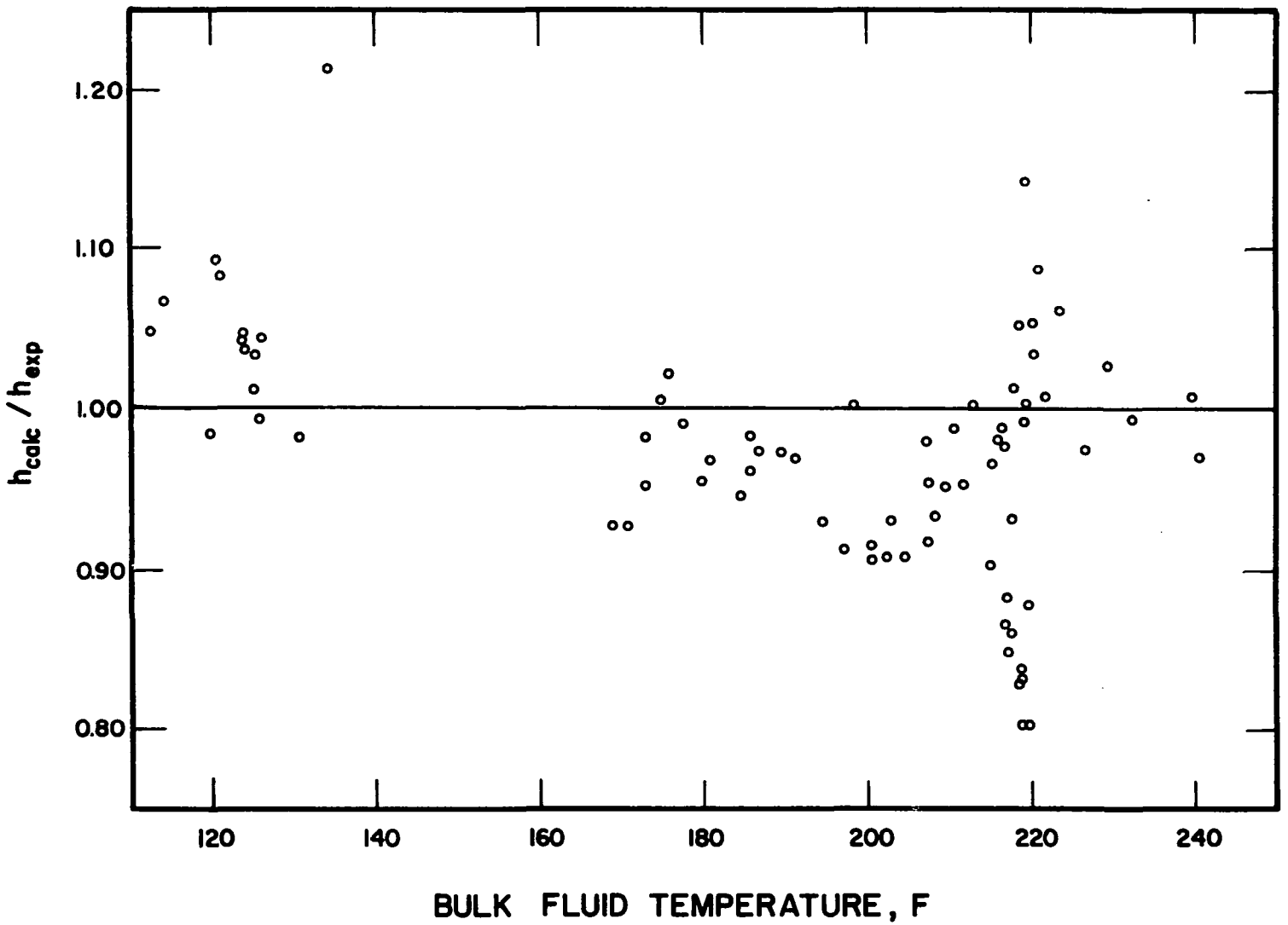

Figure 15. Correlation of Heat Transfer Data with Equation (67)

was introduced in the correlation (67).

The effect of viscosity on the heat transfer coefficient is generally small except for cases of extreme variation between the wall and bulk conditions. The conventional correlations in the form of Equation (2) incorporate the bulk-to-wall viscosity ratio to the 0.1 - 0.14 power. The usual exponent is much higher than the calculated exponent of 0.02. However, an adjustment on the viscosity exponent was not attempted because of other deficiencies in the form of the expression (67). These deficiencies are discussed below.

For turbulent heat transfer to fluids with large bulk Prandtl numbers - corresponding to supercritical fluids with bulk temperatures near the transposed critical temperature - Equation (67) reduces to the form

$$h \simeq \psi(Re_b) Pr_b^{1/3} \left(\frac{C_{pm}}{C_{pb}} \right)^{0.54} \left(\frac{\rho_b}{\rho_w} \right)^{0.27} \left(\frac{k_b}{k_w} \right)^{0.20} \left(\frac{\mu_b}{\mu_w} \right)^{0.02} \tag{68}$$

where $\psi(Re_b)$ represents a function of the bulk Reynolds number. Along the critical isobar at a position such that t_b equals the critical temperature, the bulk specific heat capacity becomes infinite and thus Equation (68) predicts a heat transfer coefficient of zero value. This is obviously not correct. If it is assumed that Equation (68) has the right form, then the exponent on the ratio containing C_{pb} must be 1/3 in order to predict a finite-nonzero coefficient at the critical pressure for t_b equal to the critical temperature. The correlation obtained by the least squares

method forcing the C_p exponent to be 1/3 was not satisfactory. Hence, the form of the expression would not accurately predict heat transfer coefficients at the critical point of a fluid. It is likely that expressions utilizing a specific heat capacity evaluated at a fixed temperature will also be inadequate in the very near-critical region

Aside from the limitation at the critical point, the correlation is obviously an oversimplification of the integration for the bulk enthalpy flux. This is apparent from Equation (31) which reduces to the form

$$h = h'_{t_b} \left(\frac{C_{pm}}{C_{pb}} \right) \frac{(H_b^+ G_b^+)_{t_b}}{H_b^+ G_b^+} \tag{69}$$

The dimensionless enthalpy flux, (26), may be expressed as

$$H_b^+ G_b^+ = \frac{2}{R^+} \int_0^{y_1^+} H^+ G^+ \left(\frac{R^+ - y^+}{R^+} \right) dy^+ + \frac{2}{R^+} \int_{y_1^+}^{R^+} H^+ G^+ \left(\frac{R^+ - y^+}{R^+} \right) dy^+ \tag{70}$$

where the subscript 1 corresponds to the position near the wall where the transition from Equation (11) to (12) occurs. The first integral is negligible since $R^+ >> y_1^+$. For constant physical properties, utilizing Deissler's assumptions listed in Chapter II and Schwarz's inequality, the integration of the second term in (70) is given by the expression

$$(H_b^+ G_b^+)_t \simeq (G_b^+)_t^2 \left\{ \left(\frac{G_1^+}{G_b^+} \right)_t \left[\left(\frac{H_1^+}{G_1^+} \right)_t - 1 \right] + 1 \right\} \tag{71}$$

where the subscript t refers to constant properties equivalent to the properties at temperature t. From the definitions of the friction factor, (17), and the dimensionless mass velocity (22), it follows that,

$$(G_b^+)_t = u_b^+ = (2/f_b)^{1/2} \tag{72}$$

and

$$(G_1^+)_t = u_1^+ \simeq 12.7 \tag{73}$$

A comparison of Equations (16), (30), (71), (72), and (73) reveals that

$$\left(\frac{H_1^+}{G_1^+}\right)_t = Pr_t^{2/3} \tag{74}$$

All of the quantities in expressions (72) through (74) are functions of property variations. The function, H_1^+/G_1^+, is more sensitive to property variations in the supercritical region since it depends on the specific heat capacity. Hence, a correlation of the form,

$$Nu_b = \frac{Re_b\ Pr_b \left(\frac{C_{pm}}{C_{pb}}\right)\left(\frac{f_b}{2}\right)}{12.7\left(\frac{f_b}{2}\right)^{1/2}\left[Pr_w^{2/3}\left(\frac{C_{pw}}{C_{pf}}\right)^{a'}\left(\frac{k_w}{k_f}\right)^{b'}\left(\frac{\rho_w}{\rho_f}\right)^{c'}\left(\frac{\mu_w}{\mu_f}\right)^{d'} - 1\right] + 1} \tag{75}$$

was investigated. The subscript f refers to film properties evaluated at the arithmetic mean of the wall and bulk temperatures. A least square fit of the exponents did not yield a satisfactory correlation. Minor modifications of the form

of (75) were also investigated but none of the forms studied were as successful as Equation (67).

The proposed equation, (67), correlates successfully local heat transfer coefficients for propane in the supercritical region even though its form appears incorrect. The major advantage of this type of correlation is that it reduces to the conventional expression when applied to regions remote from the critical state. It also apparently yields conservative estimates for heat transfer coefficients near the transposed critical state.

The applicability of the proposed equation for calculating heat transfer to other fluids in the supercritical region requires further verification.

CHAPTER VII

CONCLUSIONS

The results of an experimental investigation of heat transfer in the supercritical region of propane reveal that the relative maximum in the heat transfer coefficient as a function of either the bulk or wall fluid temperature becomes smaller and less pronounced, and is displaced further from the transposed critical temperature as the heat flux is increased. For small wall-to-bulk temperature differences, h can be correlated satisfactorily by well known equations valid at constant fluid properties. When the temperature differences are large, the heat transfer rate depends primarily on the radial variation of the properties and their derivatives.

An equation, (67), is proposed which correlates, with good approximation, local heat transfer coefficients for propane at 700 psia. The major advantages of this type of correlation are its simplicity, the fact that it reduces to a conventional expression when physical property variations are small, and that it predicts conservative values for the heat transfer coefficient near the transposed critical state.

The form of the proposed correlation is shown to be

incorrect from an analysis of the heat transfer coefficient at the critical pressure when the bulk fluid temperature equals the critical temperature. It is likely that correlations utilizing a specific heat capacity evaluated at a reference temperature will also be inadequate near the critical state.

BIBLIOGRAPHY

1. Abas-Zade, A. K., Doklady Akad. Nauk. S.S.S.R., 99, 227 (1954)

2. Anonymous, Engineering Properties of Inconel, The International Nickel Co., Inc., New York (1950)

3. API Research Project 44, Selected Values of Properties of Hydrocarbons and Related Compounds, Carnegie Institute of Technology, Pittsburgh, Penn. (October 1958)

4. Beattie, J. A., Kay, W. C., and Kaminsky, J., J. Am. Chem. Soc., 59, 1489 (1937)

5. Bringer, R. P., and Smith, J. M., A.I.Ch.E. Journal, 3, 49 (1957)

6. Canjar, L. N., Patel, N. R., and Manning, F. S., Petrol. Refiner, 41, 203 (1962)

7. Deissler, R. G., Trans. ASME, 76, (1954)

8. Deissler, R. G., NACA TN 2138 (1950)

9. Deissler, R. G., NACA TN 2629 (1952)

10. Deissler, R. G., NACA RM E53B17 (1953)

11. Deissler, R. G., NACA Report 1210 (1955)

12. Deschner, W. W., and Brown, G. G., Ind. Eng. Chem., 32, 836 (1940)

13. Dickinson, N. L., and Welch, C. P., Trans. ASME, 80, 3 (1958)

14. Din, F., ed., Thermodynamic Functions of Gases, v. 2, Butterworths, London (1956)

15. Eckert, E. R. G., J. Aero. Sci., 22, 585 (1955)

16. Goldman, Kurt, Chem. Eng. Prog. Sym. Ser. No. 11, 50, 105 (1954)

17. Griffith, J. D., and Sabersky, R. H., Jour. ARS, 30, 289 (1960)

18. Hsu, Yih-Yum, and Smith, J. M., J. Heat Transfer, 83, 176 (1961)

19. Knuth, E. L., Int. Journ. Heat and Mass Transfer, 6, 1083 (1963)

20. Knuth, E. L., Ibid., 6, 1 (1963)

21. Knuth, E. L., and Dershin, H., Ibid., 6, 999 (1963)

22. Koppel, L. B., Ph.D. thesis, Northwestern University, Evanston, Illinois (August, 1960)

23. Koppel, L. B., and Smith, J. M., International Developments in Heat Transfer, ASME, Sec. III, Paper No. 69, p.585 (1961)

24. Leng, D. E., and Comings, E. W., Ind. Eng. Chem., 49, 2042 (1957)

25. Miropolsky, Z. L., and Shitzman, M. E., Journal of Technical Physics, 27, 2359 (1957)

26. Owens, E. J., and Thodos, G., A.I.Ch.E. Journal, 3, 454 (1957)

27. Petukhov, B. S., and Kirillov, V. V., Teploenergetika, 4, 63 (1958)

28. Petukhov, B. S., Krasnoschekov, E. A., and Protopopov, V. S., International Development in Heat Transfer, ASME Sec. III, Paper No. 67, p. 569 (1961)

29. Pfenning, D. B., M.S. thesis, University of Oklahoma, Norman, Oklahoma (October, 1963)

30. Powell, W. B., Jet Propulsion, 27, 776 (1957)

31. Reamer, H. H., Sage, B. H., and Lacey, W. N., Ind. Eng. Chem., 41, 482 (1949)

32. Rubesin, H. W., and Johnson, H. A., Trans. ASME, 71, 383 (1949)

33. Sage, B. H., and Lacey, W. N., Volumetric and Phase Behavior of Hydrocarbons, Stanford University Press, Stanford University (1939)

34. Seider, E. N., and Tate, G. E., Ind. Eng. Chem., 28, 1429 (1936)

35. Shitzman, M. E., Teploenergetika, 1, 68 (1959)

36. Sommer, S. C., and Short, B. J., J. Aero. Sci., 23, 536 (1956)

37. Starling, K. E., Eakin, B. E., and Ellington, R. T., Liquid, Gas and Dense Fluid Viscosity of Propane, Unpublished paper from Institute of Gas Technology (1959)

38. Starling, K. E., M.S. thesis, Illinois Institute of Technology, Chicago, Illinois (January, 1960)

39. Wood, R. D., and Smith, J. M., A.I.Ch.E. Journal 10, 180 (1964)

40. Young, G. B. W., and Janssen, E., J. Aero. Sci., 19, 229 (1952)

NOMENCLATURE

A_c = Cross-sectional tube area available for flow, ft^2

A_i = Inside tube wall area available for heat transfer, ft^2

a = Empirical constant

b = Empirical constant

C_p = Local isobaric specific heat capacity, Btu/lbm F

C_{pb} = Isobaric specific heat capacity evaluated at bulk temperature

C_{pm} = Mean integrated specific heat capacity defined by Equation (24)

C_{pw} = Isobaric specific heat capacity evaluated at wall temperature

c = Empirical constant

D = Inside tube diameter, ft

d = Empirical constant

E = Voltage drop across test section, volts

F(x) = Even function of x in Equation (48)

f = Friction factor, defined by Equation (17)

f(x) = Odd function of x in Equation (48)

G = Local mass velocity, ρu, lbm/hr ft^2

G_b = Bulk mass velocity given by W/A_c

G^+ = Dimensionless mass velocity, defined by Equation (22)

G_b^+ = Dimensionless bulk mass velocity when $G = G_b$

g = Acceleration of gravity, ft/sec^2

g_c = Dimensional constant, 32.17 lbm ft/ lbf sec^2

$\bar{H}$ = Specific enthalpy of fluid, Btu/lbm

$\bar{H}_b$ = Bulk specific enthalpy of fluid defined by Equation (20)

$\bar{H}_w$ = Specific enthalpy evaluated at wall temperature

H^+ = Dimensionless enthalpy, defined by Equation (21)

H_b^+ = Dimensionless bulk enthalpy, defined by Equation (23)

h = Local heat transfer coefficient, Btu/hr ft^2 F

h_t' = Local heat transfer coefficient evaluated at constant fluid properties at temperature, t

J = Energy conversion factor in Equation (34)

K = Flow meter constant, pulses/gallon

k = Thermal conductivity of fluid, Btu/hr ft F

k_b = Thermal conductivity evaluated at bulk conditions

k_I = Thermal conductivity of Inconel

k_w = Thermal conductivity evaluated at wall temperature

L = Tube length in ft

m = Empirical constant in the expression for the eddy diffusivity, Equation (12)

n = Empirical constant in the expression for the eddy diffusivity, Equation (11)

Nu = Nusselt number, hD/k

Nu' = Isothermal Nusselt number

Nu_b' = Isothermal Nusselt number evaluated at t_b

P = Absolute static fluid pressure, psia

Pr = Prandtl number, $C_p\mu/k$

Pr_b = Prandtl number evaluated at bulk properties

Pr_t = Prandtl number evaluated at constant fluid properties at temperature, t

$\bar{Q}$ = Heat transferred per unit mass of flowing fluid, Btu/lbm

$\dot{Q}$ = Net rate of heat generation, Btu/hr

$\dot{Q}_l$ = Rate of heat loss from tube, Btu/hr

q = Local radial heat flux, Btu/hr ft^2

q_w = Radial heat flux evaluated at the tube wall

R = Inside tube radius, ft

R^+ = Dimensionless tube radius, defined by Equation (6) when $y = R$

Re = Reynolds number, DG/μ

Re_b = Reynolds number evaluated at bulk fluid properties

r = Radius variable, distance from tube center, ft

T = Absolute temperature, Rankine

t = Temperature, F

t_b = Bulk fluid temperature, F

t_c = Critical temperature, F

t_c' = Transposed critical temperature, F

t_s = External tube wall temperature observed with thermocouple, F

t_w = Inside tube wall temperature, F

t^+ = Dimensionless temperature, defined by Equation (7)

u = Local fluid velocity in axial direction, ft/sec

u^+ = Dimensionless velocity, defined by Equation (5)

u_b^+ = Dimensionless bulk velocity

v = Bulk fluid velocity, ft/sec

v_* = Shear velocity, defined by Equation (8)

$\bar{W}$ = Work transferred per unit mass of flowing fluid, Btu/lbm

w = Mass flow rate, lbm/hr

x = Parameter defined as $(t - t_c')$, F

y = Perpendicular distance from tube wall, ft

y^+ = Dimensionless distance from tube wall, defined by Equation (6)

Z = Elevation above an arbitrary datum level, ft

z = Axial length variable measured from tube entrance, i.e., distance from point of power application, ft

β = Dimensionless heat transfer parameter, defined by Equation (7)

Δ = Linear operator, defined as output minus input

δ = Error

ϵ_m = Eddy diffusivity of momentum, ft^2/hr

ϵ_h = Eddy diffusivity of heat transfer, ft^2/hr

μ = Viscosity, lbm/ft hr

μ' = Joule-Thomson coefficient, F/psia

μ_b = Viscosity evaluated at bulk temperature

μ_w = Viscosity evaluated at wall temperature

ξ = Ratio of outside-to-inside tube radii

ρ = Density, lbm/ft^3

ρ_b = Density evaluated at bulk temperature

ρ_w = Density evaluated at wall temperature

σ = $H - H'_{t_c}$, Btu/lbm

τ = Shear stress, lbf/ft^2

τ_w = Shear stress at tube wall

φ = Functional notation

Ψ = Any of the physical and transport properties in Equation (13)

Ω = Tube electrical resistance, ohms

Subscripts

b = Bulk conditions

c = Critical state

f = Film conditions, evaluated at the arithmetic mean of the wall and bulk temperature

I = Conditions at tube entrance

O = Conditions at tube exit

t = Conditions corresponding to constant fluid properties evaluated at temperature, t

w = Wall conditions

0 = Absolute zero reference temperature

1 = Position of transition from Equation (11) to (12)

Superscripts

c = Crystalline state

O = Ideal gas state

APPENDIX I

Calibrations

Fluid Thermocouple Calibrations

The fluid thermocouples, located in the inlet and exit mixing chambers and downstream from the flowmeter, were calibrated to 0.02F against a platinum resistance thermometer. The thermometer and thermocouples were placed in a well-agitated constant temperature bath of triethylene glycol. The bath assembly consisted of a 9 liter silvered dewar flask with a wooden top and a variable-speed agitator. Temperature control of the bath was accomplished with a Bayley proportional controller with a 25 watt control heater. The resistance of the platinum thermometer was determined with a Leeds and Northrup Mueller bridge accurate to ±0.00001 ohms. The thermocouple EMF's were measured with a Leeds and Northrup precision potentiometer, Model K2, accurate to 0.0002 MV.

The thermocouples were calibrated from 95 - 340F in approximately 40F intervals. The results of the calibration are shown in Figure 16.

Test Section Resistance Calibration

The electrical resistance of the test section was determined by the potentiometric method. The accuracy of this method was checked by measurements using the Mueller bridge at two temperatures. The agreement between the two methods was excellent: ±0.00001 ohms. The resistance measuring circuit consisted of a 6 volt source and three resistances in series - a 0.01 ohm precision resistor, the test section, and a variable resistance for controlling the

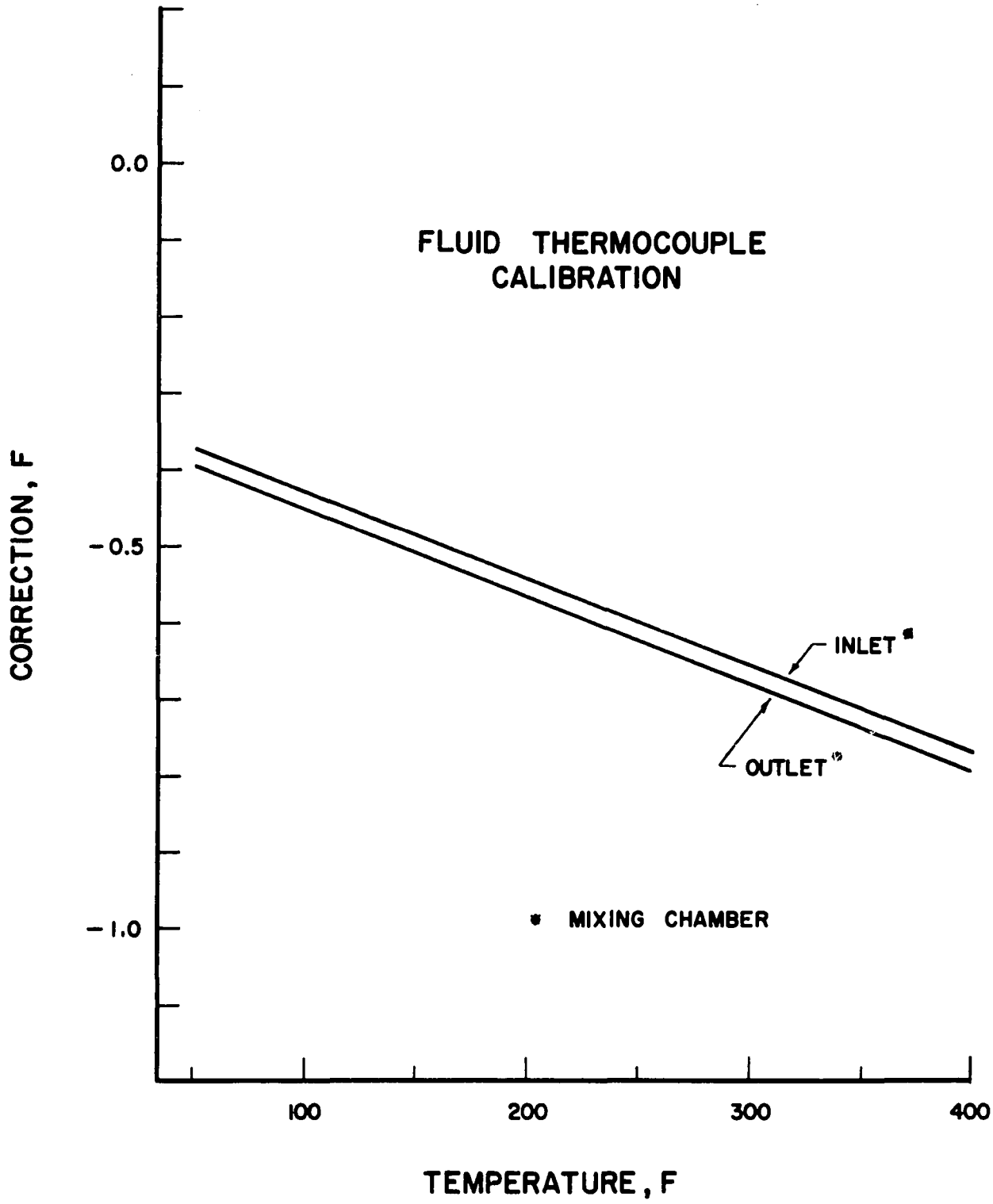

Figure 16. Fluid Thermocouple Calibration

potential drop across the known resistance. The EMF measurements across the standard resistance and the test section were made with a Leeds and Northrup precision potentiometer, Model 8662.

The calibration was accomplished by circulating propane adiabatically through the insulated tube and measuring the potential drop across the standard resistor and the test section. The resistance of the test section was calculated from the expression

$$\Omega_{tube} = 0.01 \frac{E_{tube}}{E_{0.01}} \qquad (I\text{-}1)$$

where E refers to the measured EMF. The temperature of the test section was determined from measurements of the bulk fluid temperature at the inlet and exit mixing chambers. The results of the calibration are shown in Figure 17. The maximum temperature that could be achieved by this method was 275F. For heat transfer runs at higher wall temperatures, the resistance was obtained by linear extrapolation of the calibration curve.

Tube Heat Loss Calibration

The tube heat losses were determined by supplying electrical energy to the test section with the heat transfer loop under a vacuum. A typical wall temperature profile for one of these tests is shown in Figure 18. The relative flatness of the profile in the central portion of the tube indicates that conduction losses from the ends of the tube are

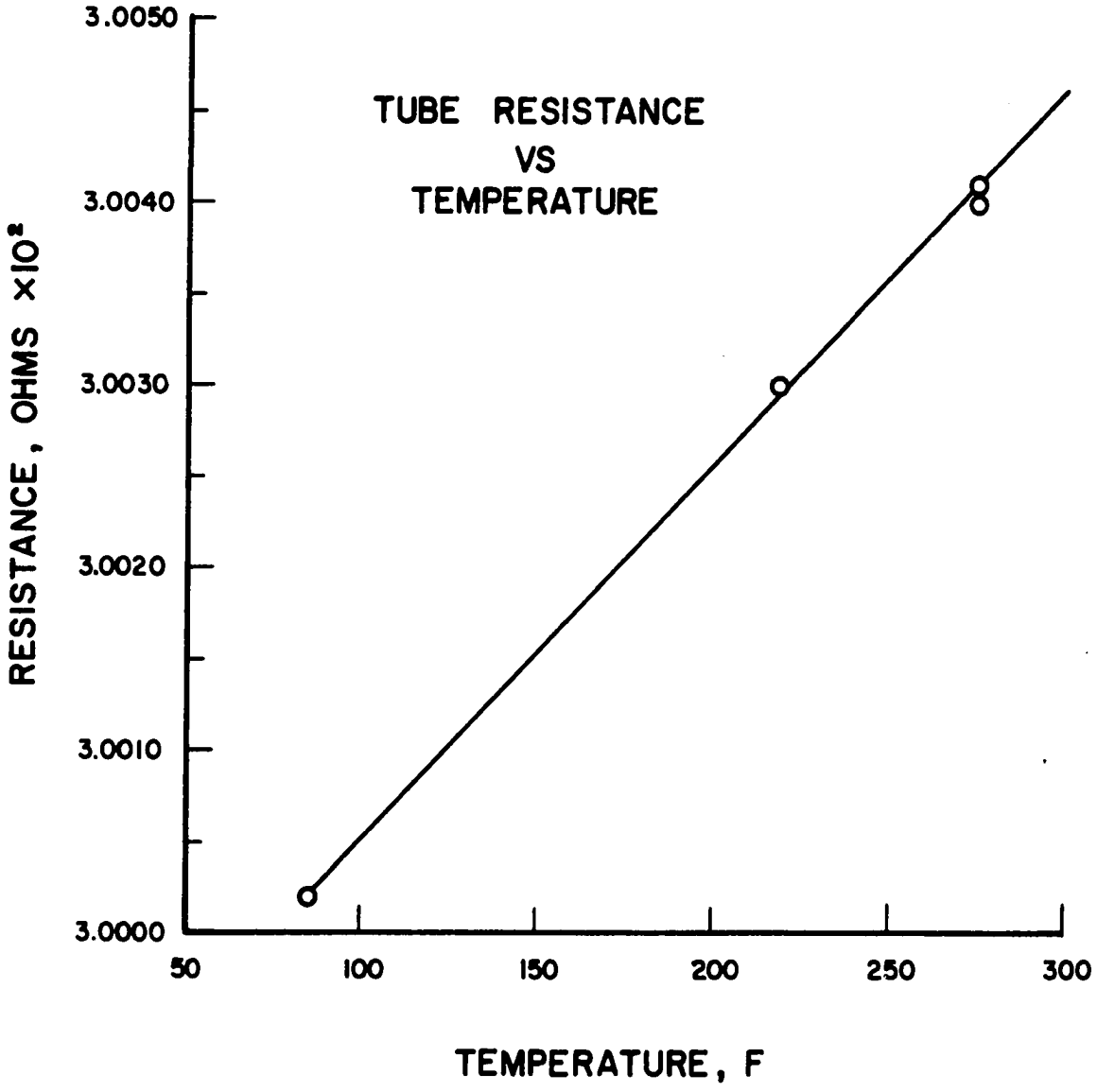

Figure 17. Resistance Calibration of Test Section

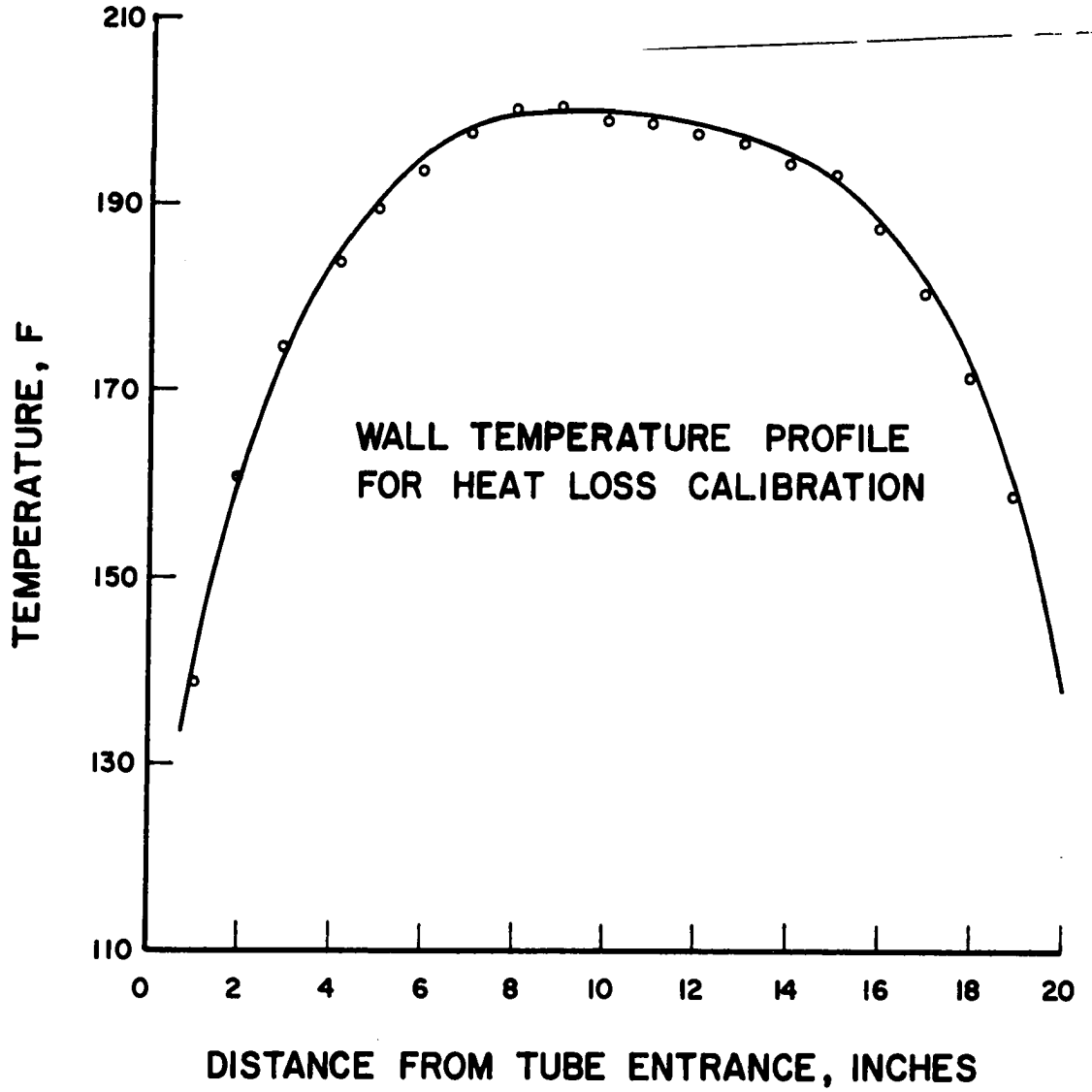

Figure 18. Wall Temperature Profile - No Flow Condition

small and would not affect the profile in the center of the tube in actual heat transfer tests.

The electrical power dissipation necessary to maintain the central portion of the tube at various temperature levels is summarized in Table IV and plotted in Figure 19. The heat losses were linear with wall temperature.

Flowmeter Calibration

The Waugh turbine flow meter was calibrated in place using water by measuring the number of pulses recorded on the scaler, the amount of water collected, and the observation period. The results of the calibration, tabulated in Table V, show that the meter has an accuracy of 0.3%.

From dimensional analysis it can be shown that the volumetric flow rate through the meter is a function of the ratio of the signal frequency to the kinematic viscosity of the flowing fluid. Since propane in the supercritical region at 700 psia has a kinematic viscosity of 1/5 to 1/10 that of water, the meter calibration was checked in a region removed from the transposed critical state. The meter constant was calculated from the overall energy balance using the enthalpy data of Din (14) by the relation

$$w = \frac{\dot{Q}}{\Delta \bar{H}_b} = \frac{3600f}{K} \left(\frac{\text{lbm}}{\text{gal}} \right) \qquad (I\text{-}2)$$

where f is the meter signal frequency in cps and K is the constant in pulses/gal. Results of the calibration are shown in Figure 20. As indicated from dimensional considerations,

TABLE IV

HEAT LOSSES AS A FUNCTION OF TUBE WALL TEMPERATURE

Central tube wall temperature, F	Electrical Power Dissipation, watts	Heat Loss, Btu/hr
199	5.8	19.9
300	12.1	41.3
361	16.3	55.6

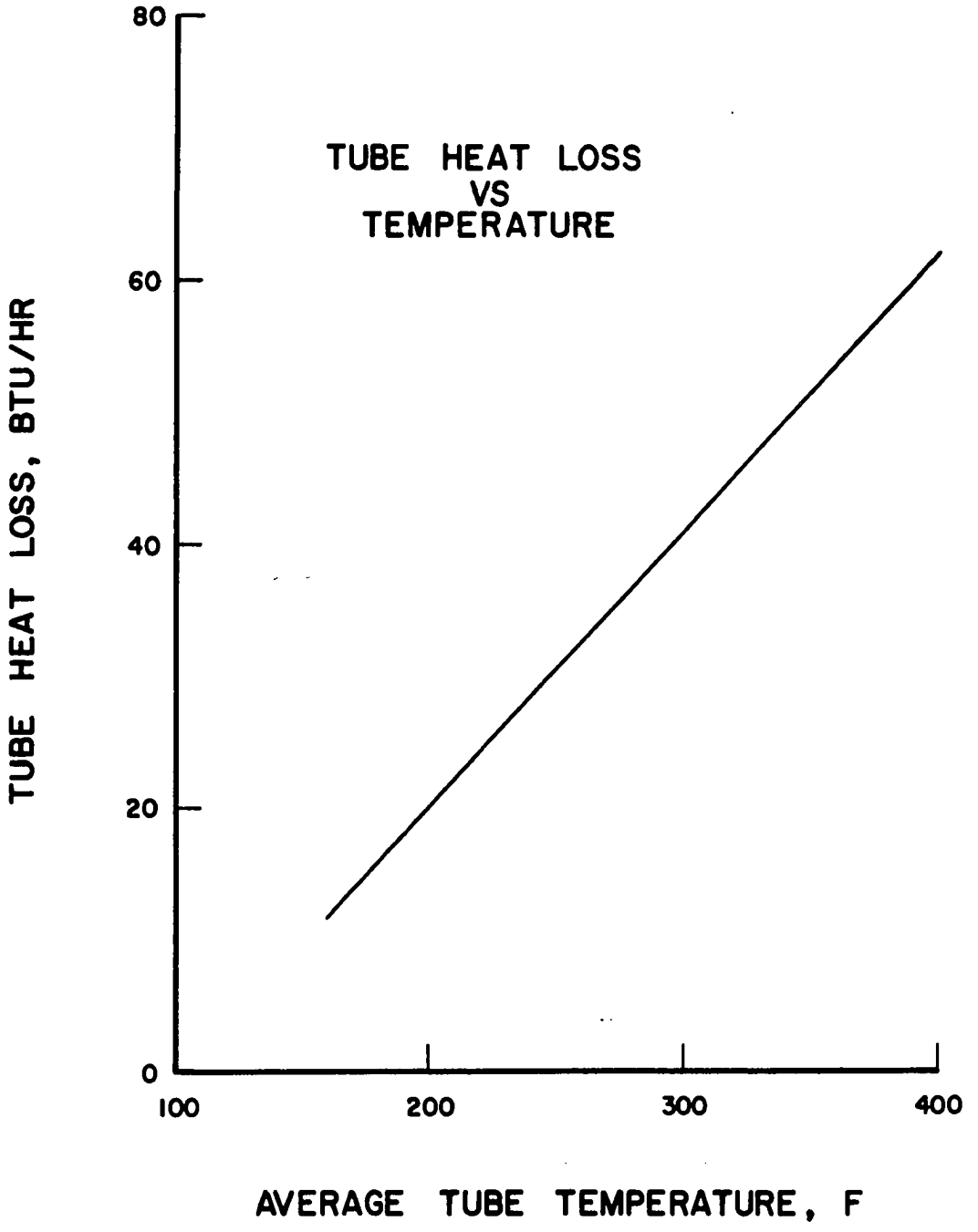

Figure 19. Tube Heat Loss Calibration

TABLE V

TURBINE FLOWMETER CALIBRATION

Test Fluid - Water

Flow Rate, gpm	Meter Signal Frequency, cps	Meter Constant, pulses/gallon
3.106	173.42	3349
3.105	173.29	3348
2.546	141.85	3343
1.988	110.91	3347
1.420	79.36	3353
1.383	77.26	3352
1.081	60.61	3363
0.898	50.31	3360
0.879	49.25	3361

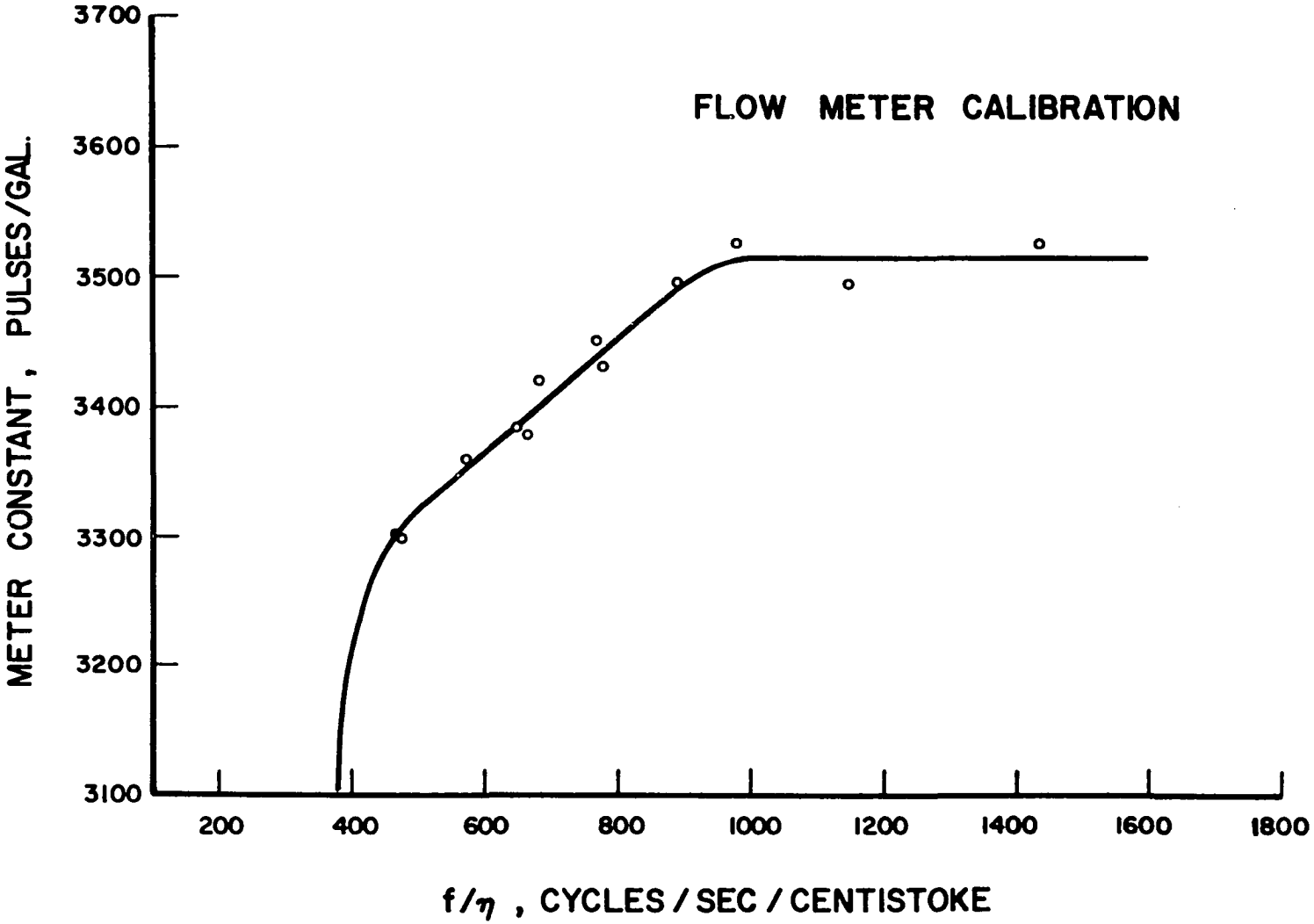

Figure 20. Flowmeter Calibration

the results are different than those obtained using water, Table V. The propane calibration was used to determine the mass flow rate for all runs with an accuracy of 0.6%.

APPENDIX II

Experimental Heat Transfer Data

TABLE VI

EXPERIMENTAL AND CALCULATED DATA

Thermocouple readings are inside wall temperatures in F; location of thermocouples is given in Table VII. Values reported for h_{11} are heat transfer coefficients at a point 11 in. from the upstream point of electrical power application.

EXPERIMENTAL AND CALCULATED HEAT TRANSFER DATA

Run	Thermocouple Number 2	3	4	5	6	7	8	9
1c	192.9	197.6	202.7	206.9	208.6	209.9	211.4	211.1
2c	170.8	174.5	178.6	180.6	181.8	183.9	186.0	187.3
3c	193.9	198.3	203.3	204.4	206.1	208.4	209.8	211.5
4c	160.9	164.2	167.5	169.5	170.6	171.5	173.2	174.7
5c	190.5	194.3	198.1	199.9	202.0	204.1	204.8	206.6
6c	188.3	189.9	195.0	197.6	199.4	200.7	201.9	203.1
7c	189.5	193.9	198.7	200.9	203.8	204.8	207.6	208.7
8c	231.6	241.8	253.0	261.3	271.8	281.3	290.6	300.4
9c	196.6	201.2	205.7	207.5	209.6	211.5	213.5	215.0
10c	201.6	205.0	210.2	212.6	214.1	215.9	217.8	218.7
11c	194.8	199.0	202.4	204.5	206.8	209.3	209.5	212.0
12c	205.3	208.4	211.9	215.1	216.5	218.1	218.9	220.3
13c	177.8	180.4	180.5	185.6	187.9	188.6	189.9	191.4
14c	207.8	211.4	215.9	218.1	220.0	221.3	222.3	224.0
1	177.6	178.3	178.7	178.9	179.3	179.8	179.9	180.1
2	185.0	185.9	186.7	187.1	187.6	188.9	188.9	188.9
3	194.2	195.3	196.5	197.0	197.5	199.1	199.6	199.8
4	201.0	202.6	204.3	204.9	205.4	206.4	206.6	207.2
5	214.3	215.4	218.1	218.8	219.8	220.5	221.1	221.4
6	224.9	227.0	229.2	231.0	232.8	235.1	235.3	236.4
13	204.4	206.0	207.7	208.4	208.2	209.9	210.8	211.0
14	218.8	220.7	222.5	223.6	224.5	225.9	226.5	228.0
15	230.6	234.9	238.7	240.2	242.6	246.3	247.3	248.9
16	267.5	279.2	286.3	289.8	290.0	292.8	294.0	294.4
49	232.7	237.1	241.1	243.5	245.2	248.3	249.3	251.9
50	239.0	246.0	251.7	254.2	256.6	258.8	258.6	260.3
51	248.0	257.1	264.9	267.6	270.7	273.0	274.2	275.1
52	251.4	259.8	265.2	268.6	269.9	272.0	272.7	274.2
53	242.1	248.3	253.5	257.2	259.4	261.1	262.2	263.8
54	248.2	253.2	258.1	260.6	262.1	266.5	264.7	264.8
55	244.9	248.0	251.5	253.2	254.0	255.3	255.7	256.8
56	269.6	274.1	277.3	279.1	278.9	280.8	281.3	282.0
57	272.2	274.4	277.9	278.9	279.5	280.9	282.1	282.5
58	275.8	277.5	279.8	280.8	281.6	283.4	283.4	284.9
59	269.7	272.9	276.5	277.6	277.9	278.8	279.2	280.7
60	265.6	271.9	275.6	277.2	278.4	279.5	279.5	280.3
62	306.6	309.1	313.3	316.1	317.9	321.1	324.5	328.1
63	306.8	309.9	312.6	317.0	317.6	320.0	323.0	325.8
64	285.3	287.1	291.5	295.2	297.8	299.4	302.5	302.5
65	285.1	287.2	290.8	293.0	294.9	297.8	299.5	302.2
66	286.2	289.4	293.5	295.9	298.1	301.6	305.8	307.7
67	304.4	309.5	315.6	319.4	323.4	327.7	331.1	336.0
68	324.8	332.6	341.0	346.4	351.1	357.7	363.0	369.6
73	296.4	301.7	308.0	311.1	314.9	318.7	321.8	325.7
74	288.4	290.0	292.6	294.9	295.5	296.9	298.4	299.7

Run	Thermocouple Number 2	3	4	5	6	7	8	9
75	289.8	290.8	294.2	295.9	296.5	298.9	300.3	301.9
76	294.3	298.9	305.3	308.2	309.8	314.0	317.2	320.5
77	302.8	309.9	316.7	320.6	322.9	327.6	327.3	334.2
79	306.1	313.2	319.9	324.2	329.4	333.3	336.0	339.9
81	281.1	282.1	285.7	287.6	287.3	289.1	290.4	292.4
82	286.2	287.9	290.4	292.0	293.6	294.9	296.2	298.1
84	279.7	281.0	283.7	286.3	287.8	289.2	290.7	292.0
85	281.6	282.8	286.7	288.6	289.6	292.2	294.4	296.6
86	285.8	287.9	292.6	294.6	296.7	299.3	301.7	304.5
87	290.2	293.9	299.5	302.4	305.4	308.6	311.2	314.4
88	300.5	306.0	312.2	315.9	319.5	323.5	326.7	326.2
89	302.8	309.4	315.1	318.1	321.4	324.5	325.8	327.8
90	325.1	333.9	341.9	344.6	348.7	352.7	354.9	356.9
91	318.2	325.9	332.9	332.5	339.8	342.7	345.7	348.1
94	282.3	284.9	290.4	293.0	295.3	297.2	298.7	300.4
95	293.5	297.3	303.2	305.9	308.7	312.0	313.6	315.6
96	294.1	299.3	304.2	307.1	309.6	312.9	314.5	316.9
97	288.5	293.6	297.8	300.9	303.1	305.8	307.9	310.4
98	278.3	282.0	286.7	290.2	292.9	294.4	296.0	298.0
100	282.9	284.6	289.7	292.2	293.2	295.7	296.0	297.2
101	219.4	219.3	220.5	220.6	221.2	222.4	222.1	222.5
102	227.3	227.3	228.4	228.4	228.8	229.3	229.5	229.8
103	233.5	233.8	234.7	234.6	234.8	235.8	235.8	236.4
104	229.2	229.2	229.8	229.9	230.2	231.1	230.8	231.1
105	227.6	227.6	228.2	228.0	228.4	229.0	229.0	229.3
106	253.7	258.4	262.8	264.1	265.8	267.1	268.1	269.0
107	305.7	312.2	319.3	323.7	326.2	331.9	335.2	338.5
109	365.1	378.9	391.8	401.3	410.4	421.8	432.8	444.9
110	341.2	352.2	360.7	368.1	375.2	383.8	392.1	400.6
111	224.5	224.6	224.7	224.3	224.6	225.3	225.1	225.4
112	248.3	249.2	250.9	250.9	251.6	253.1	253.3	254.8
115	226.1	226.0	226.5	226.4	226.6	227.3	227.1	227.4
116	224.9	224.7	225.2	225.0	225.5	226.0	226.0	226.4
117	222.1	221.9	223.0	221.9	222.2	223.0	222.7	222.9
118	222.3	222.2	222.4	222.2	222.2	222.7	222.5	222.7
120	222.3	222.2	222.4	222.2	222.2	222.7	222.5	222.7
121	222.7	222.5	222.7	222.5	222.6	223.4	223.3	223.3
122	221.0	220.9	221.1	220.8	220.9	221.8	221.5	221.8
124	245.0	246.4	248.0	248.2	249.5	250.5	250.3	250.7
125	218.8	218.8	218.9	218.6	218.8	219.5	219.2	219.5
126	221.5	221.4	221.5	221.3	221.3	222.2	221.7	221.9
127	223.3	223.2	223.4	223.2	223.1	224.2	224.1	224.2

Run	Thermocouple Number 10	11	12	13	14	15	16	17
1c	215.6	216.3	217.1	218.4	219.0	219.7	221.1	222.2
2c	189.6	190.1	191.3	192.7	193.0	194.0	195.8	197.2
3c	213.8	214.2	215.1	216.1	216.3	217.6	219.0	219.9
4c	176.2	177.0	178.1	179.1	179.7	180.5	181.7	183.1
5c	208.7	209.0	209.9	210.7	211.1	212.4	213.8	214.3
6c	205.1	205.2	205.9	206.9	207.3	208.7	210.1	211.9
7c	210.4	212.1	213.4	214.8	215.7	216.5	218.0	219.3
8c	313.3	320.8	323.6	327.5	328.2	330.0	334.4	335.9
9c	216.8	217.6	218.1	219.3	219.8	220.2	221.5	222.7
10c	220.1	220.5	221.3	222.2	222.6	223.4	224.8	226.0
11c	213.9	214.3	215.1	216.2	216.6	217.4	218.8	219.4
12c	221.9	222.3	222.7	224.7	224.8	225.8	227.7	228.8
13c	193.0	193.5	194.5	196.7	196.8	197.8	198.9	200.0
14c	225.9	226.4	227.1	228.8	229.2	230.6	233.1	235.0
1	180.4	180.4	180.9	181.1	181.5	181.8	182.0	182.3
2	189.5	189.5	190.0	189.9	189.9	190.2	190.6	191.0
3	200.5	200.6	201.2	201.3	201.2	201.6	202.2	202.5
4	208.3	208.4	209.4	209.9	210.3	210.7	211.4	211.8
5	222.6	223.0	223.4	223.5	223.7	224.8	225.2	225.6
6	238.0	239.1	239.3	239.9	240.2	242.6	244.7	246.3
13	211.6	212.0	212.4	212.5	212.8	213.2	214.0	214.6
14	228.2	228.8	229.7	230.3	230.5	231.1	232.4	233.2
15	252.1	253.6	254.0	255.6	255.6	258.4	260.5	262.0
16	296.2	298.0	297.4	298.4	298.4	301.3	302.5	303.8
49	254.7	255.6	255.3	256.7	257.4	260.1	261.4	262.4
50	263.6	263.2	263.1	264.1	264.4	266.1	268.0	268.7
51	278.3	279.2	279.1	279.6	279.8	281.2	282.9	283.8
52	276.6	276.5	276.5	276.8	277.2	278.4	279.9	280.0
53	266.2	266.4	266.0	266.8	266.7	268.7	270.1	270.5
54	267.3	267.3	266.9	267.2	268.0	269.0	270.5	271.1
55	258.5	258.1	257.9	258.6	258.9	259.6	260.4	260.8
56	283.4	284.0	283.9	283.3	283.6	288.7	287.2	287.5
57	284.4	284.6	284.0	284.7	284.7	285.6	287.0	288.0
58	286.6	287.1	286.9	288.2	288.3	289.9	291.2	292.2
59	282.8	282.5	282.3	283.0	283.2	284.6	286.2	287.9
60	282.4	282.5	282.4	283.0	283.0	284.0	285.6	285.7
62	332.8	336.1	337.9	341.8	345.7	350.1	357.5	357.7
63	330.2	334.1	334.5	339.2	339.6	343.2	348.8	350.5
64	305.4	306.9	308.0	311.1	312.2	314.5	316.9	318.0
65	305.9	307.1	308.1	309.4	311.5	313.9	316.9	317.8
66	311.0	313.0	314.0	317.3	320.5	321.8	324.5	324.7
67	340.3	342.0	343.7	348.0	351.5	354.5	358.5	359.2
68	377.2	380.1	381.7		390.2	394.2	398.4	399.5
73	329.0	330.5	332.8	337.6	340.2	342.3	342.3	343.8
74	302.8	304.2	304.7	306.6	307.6	309.2	312.0	313.3
75	303.9	305.7	305.7	307.4	308.6	310.0	314.5	315.6
76	323.9	325.3	327.1	330.7	332.4	334.9	337.7	339.3

Run	Thermocouple Number 10	11	12	13	14	15	16	17
77	338.1	341.2	342.0	345.3	347.5	348.6	351.9	353.4
79	342.9	345.9	347.1	350.0	352.8	354.0	356.6	358.0
81	296.0	297.3	296.8	299.0	299.4	300.5	302.8	303.9
82	301.3	303.0	303.6	306.1	307.7	309.6	312.3	313.5
84	294.7	295.1	295.3	297.4	299.4	300.7	303.4	304.3
85	299.2	299.4	300.4	302.8	304.1	305.7	309.0	309.3
86	308.3	309.2	310.3	312.7	315.3	317.4	319.2	320.8
87	318.0	318.5	320.0	323.6	325.5	327.4	330.1	331.6
88	333.7	335.5	337.2	240.4	343.2	346.2	347.3	349.4
89	330.0	331.5	333.1	334.1	335.5	337.0	338.7	341.7
90	360.3	362.3	366.1	367.5	370.6	372.2	373.7	375.8
91	350.0	352.5	354.8	356.5	357.9	360.1	361.6	364.1
94	302.5	302.7	303.7	304.9	305.6	306.7	307.6	309.8
95	316.7	317.4	319.1	320.7	321.0	322.7	323.7	325.4
96	319.0	320.1	321.6	323.0	323.8	325.8	327.0	328.9
97	312.9	313.4	314.1	316.4	317.7	318.7	319.5	321.7
98	299.4	299.9	301.2	302.1	303.4	304.8	305.8	307.2
100	298.3	298.0	297.6	298.8	298.3	298.8	300.9	301.3
101	222.7	222.9	223.2	223.3	223.1	223.4	223.6	223.7
102	230.3	230.2	230.7	231.1	231.4	231.4	231.5	231.9
103	236.9	236.6	237.4	237.8	237.9	238.3	238.4	239.2
104	231.4	231.1	231.6	231.6	231.6	231.9	232.1	232.4
105	229.3	229.1	229.7	229.8	229.9	230.0	230.0	230.5
106	271.3	270.7	270.3	271.2	271.2	272.1	273.3	274.2
107	342.7	343.3	347.8	350.3	354.9	357.2	359.2	362.4
109	457.0	459.5	458.5	469.4	473.7	470.2	469.1	*
110	409.0	413.9	413.9	424.1	429.4	420.2	*	*
111	225.4	225.5	225.8	226.4	226.3	224.3	*	*
112	255.9	256.2	255.6	257.1	257.9	259.4	*	*
115	227.9	227.6	227.7	228.1	228.1	226.3	*	*
116	226.6	226.6	230.2	226.8	227.0	225.3	*	*
117	223.1	222.7	222.4	222.8	222.9	220.7	*	*
118	222.9	222.7	222.9	223.3	223.3	221.2	*	*
120	224.5	224.1	224.2	224.5	224.7	222.6	*	*
121	223.3	222.7	222.8	223.0	222.9	220.6	*	*
122	221.8	221.4	221.1	221.5	221.4	219.3	*	*
124	251.8	251.2	251.2	252.5	252.9	*	*	*
125	219.6	219.2	219.4	219.7	219.4	*	*	*
126	221.9	221.7	221.7	221.8	222.0	*	*	*
127	224.1	223.8	223.9	224.0	223.9	*	*	*

* No Thermocouple Signal

Run	Thermocouple Number 18	19	20	21	Inlet t_b, F	Outlet t_b, F	ΔP, psi
1c	223.4	224.8	226.0	227.1	101.9	135.8	0.43
2c	197.8	198.7	199.5	201.1	99.2	126.7	0.43
3c	220.6	221.7	222.5	223.0	106.5	138.3	0.82
4c	183.7	184.9	185.7	186.8	100.0	123.2	0.84
5c	214.7	216.4	217.8	219.2	108.5	137.4	1.32
6c	212.2	213.4	214.2	215.3	110.8	137.2	2.00
7c	220.0	221.0	222.2	223.7	102.8	136.6	0.32
8c	339.6	337.3	339.2	341.1	109.6	154.3	0.29
9c	223.3	224.7	225.9	227.2	105.6	139.0	0.60
10c	226.5	227.9	229.9	231.1	107.9	141.3	0.73
11c	220.0	220.9	221.7	222.5	108.4	139.2	1.01
12c	229.8	231.0	232.2	233.4	113.3	145.4	1.46
13c	200.1	201.3	202.4	203.5	106.9	130.9	3.30
14c	236.4	238.3	239.9	241.2	106.6	141.8	1.04
1	182.3	182.5	182.8	183.0	166.4	170.9	0.90
2	191.1	191.2	191.4	192.0	167.2	173.7	0.88
3	202.5	202.7	203.2	203.8	168.1	177.5	0.89
4	212.0	212.3	212.9	213.9	166.2	178.9	0.90
5	226.0	226.5	226.3	227.0	167.1	184.2	0.89
6	246.3	247.0	244.4	243.9	168.5	189.0	0.83
13	215.0	215.5	215.7	215.9	168.5	181.5	0.82
14	233.5	234.2	233.9	234.4	168.1	186.7	0.81
15	262.9	263.7	260.7	260.0	168.4	191.2	0.77
16	303.6	303.6	302.4	301.9	169.4	197.6	0.76
49	261.7	262.3	259.3	258.6	172.1	193.6	1.07
50	267.9	267.1	265.6	264.4	172.5	194.3	0.97
51	283.3	283.5	283.0	282.1	172.5	196.6	0.74
52	280.0	279.5	279.2	278.8	179.2	201.0	0.81
53	270.1	270.2	268.7	267.2	178.1	198.5	0.99
54	270.8	270.4	268.7	267.5	184.2	203.2	1.01
55	260.5	260.3	258.5	257.4	191.6	207.2	1.35
56	287.8	289.0	289.9	290.9	189.3	208.5	0.84
57	288.7	289.1	289.7	290.2	193.7	211.0	0.87
58	292.8	294.0	294.2	294.4	197.5	213.1	0.90
59	287.8	287.7	288.6	289.4	191.1	209.7	0.81
60	286.0	286.0	285.7	285.4	185.6	206.2	0.79
62	364.9	369.9	375.4	382.4	203.6	217.3	0.94
63	355.4	357.3	360.5	366.9	199.5	216.0	0.83
64	320.7	323.9	325.9	327.9	210.7	218.4	0.99
65	320.8	322.1	324.8	327.7	212.0	218.7	1.03
66	327.7	330.3	332.2	334.1	214.4	220.0	1.07
67	362.4	366.2	368.6	371.1	214.6	220.8	1.14
68	406.6	407.6	409.8	413.7	215.8	222.3	1.19
73	347.3	349.9	352.1	354.4	216.9	222.8	1.24
74	315.7	318.7	321.6	323.8	194.2	212.4	0.83
75	318.3	321.1	324.1	327.0	197.3	214.1	0.86

Run	Thermocouple Number 18	19	20	21	Inlet t_b, F	Outlet t_b, F	ΔP, psi
76	341.3	344.5	343.7	342.4	216.2	221.6	1.18
77	354.2	356.8	356.7	357.3	219.2	228.9	1.34
79	360.8	362.0	363.9	365.3	219.6	230.1	1.37
81	306.3	308.7	310.9	312.1	200.5	214.7	0.83
82	315.8	320.4	322.7	324.0	203.7	216.3	0.88
84	306.3	309.6	311.8	314.3	206.1	216.8	0.97
85	312.8	314.6	316.6	318.9	208.8	217.9	1.02
86	324.8	326.9	329.5	333.4	212.8	219.3	1.10
87	335.2	336.8	339.5	342.1	216.6	221.8	1.24
88	352.9	356.6	359.3	362.1	217.4	223.4	1.29
89	341.9	343.9	345.2	346.8	229.4	251.8	1.99
90	376.5	378.4	379.9	381.0	228.3	256.2	2.13
91	364.6	366.7	367.9	369.1	227.8	253.0	2.13
94	310.0	311.6	312.5	313.3	226.1	240.9	2.23
95	325.9	328.4	328.2	329.9	230.7	249.9	2.18
96	330.1	330.8	332.0	333.5	223.7	238.9	2.24
97	322.4	324.4	325.7	327.5	223.3	237.4	2.23
98	308.6	308.7	309.5	310.7	223.0	233.4	2.44
100	300.6	301.6	301.1	301.3	181.1	204.9	1.35
101	223.4	224.4	224.5	224.5	193.7	202.1	1.48
102	231.8	232.0	231.9	231.3	209.5	214.7	1.56
103	239.0	238.9	238.0	238.9	218.5	220.5	2.12
104	232.3	232.7	232.0	231.3	218.3	219.5	3.59
105	230.2	230.3	230.3	230.3	216.9	218.4	3.35
106	273.2	273.3	273.2	274 0	186.5	204.8	0.99
107	368.3	371.2	372.1	373.5	218.3	225.3	1.24
109	483.3	489.6	491.6	493.1	216.1	226.4	0.90
110	442.1	445.6	447.6	450.8	215.8	223.9	0.84
111	226.6	226.7	226 5	226.1	214.1	216.4	3.59
112	260.8	261.1	261.7	262.2	214.7	219.0	0.69
115	228.5	228.5	228.9	228.8	216.0	218.2	0.71
116	227.5	227.7	227.8	227.7	213.7	216.6	0.68
117	222.3	222.9	222.8	222.8	214.4	215.9	1.67
118	223.4	223.5	223.6	223.6	216.4	217.7	1.81
120	224.7	224.9	224.8	224.6	219.4	219.9	3.57
121	222.9	222.9	222.8	222.7	218.4	218.7	3.56
122	221.4	221.5	221.4	221.2	216.4	216.8	3.59
124	254.4	255.1	253.2	251.9	217.6	220.1	3.59
125	219.7	219.7	219.7	219.7	213.8	215.1	0.70
126	221.7	221.7	221.6	221.5	217.1	217.8	0.74
127	223.8	223.9	223.8	223.6	219.0	219.6	0.78

Run	q_w, Btu/hr-ft^2	W, lb/hr	P, psia	h_{11}, Btu/hr-ft^2-F
1c	65,070	387.6	700	671
2c	51,570	388.4	700	666
3c	84,840	530.6	700	926
4c	60,290	542.7	700	918
5c	97,210	669.3	700	1,131
6c	112,050	843.0	700	1,382
7c	55,560	331.8	700	601
8c	80,820	345.8	700	426
9c	76,550	456.6	700	810
10c	85,820	506.2	700	900
11c	93,120	598.1	700	1,033
12c	117,470	706.8	700	1,274
13c	127,750	1,080.5	700	1,706
14c	105,510	591.1	700	1,040
1	12,970	495.6	700	1,080
2	20,480	494.7	700	1,057
3	29,580	493.9	701	1,041
4	39,290	500.7	700	1,076
5	53,630	498.7	700	1,129
6	67,570	498.8	700	1,136
13	39,860	496.6	700	1,063
14	58,470	494.7	700	1,123
15	73,100	491.0	700	999
16	95,600	491.9	700	854
49	82,810	571.0	700	1,169
50	81,520	545.2	700	1,047
51	80,540	478.3	700	870
52	79,570	495.4	700	934
53	80,950	543.5	700	1,060
54	81,420	539.0	700	1,123
55	81,300	609.0	700	1,408
56	82,120	481.7	700	983
57	81,790	478.1	700	1,027
58	82,250	474.6	702	1,033
59	80,980	475.6	700	1,009
60	82,600	477.8	700	967
62	98,870	437.3	700	790
63	99,060	441.5	700	798
64	81,470	428.0	700	883
65	80,810	425.5	700	881
66	79,590	414.2	700	828
67	92,120	410.2	700	735
68	101,720	405.9	700	626
73	87,100	402.8	699	769
74	88.900	452.2	699	901
75	89,060	449.4	700	914
76	87,640	420.5	700	811

Run	q_w, Btu/hr-ft^2	w, lb/hr	P, psia	h_{11}, Btu/hr-ft^2-F
77	88,440	387.9	700	738
79	89,160	381.5	700	719
81	83,340	455.7	700	955
82	83,600	435.7	700	910
84	82,380	452.4	700	999
85	82,160	445.7	700	957
86	83,980	437.2	700	900
87	84,310	424.5	700	836
88	92,070	422.4	700	785
89	80,790	409.0	700	872
90	100,930	425.4	700	809
91	97,100	428.9	700	844
94	75,330	490.7	700	1,053
95	74,220	429.5	700	946
96	87,600	469.3	700	951
97	85,870	474.8	700	1,004
98	81,350	504.0	700	1,100
100	122,460	636.8	700	1,189
101	44,330	630.9	700	1,776
102	44,000	604.9	700	2,348
103	43,110	595.1	700	2,363
104	44,820	802.7	700	3,490
105	44,130	817.9	700	3,619
106	82,480	536.5	700	1,117
107	92,160	408.9	700	726
109	107,670	336.3	700	452
110	97,680	340.0	700	503
111	43,720	906.7	700	4,048
112	44,960	366.2	700	1,165
115	20,970	373.1	700	1,953
116	21,170	375.7	700	1,389
117	21,150	586.8	700	2,896
118	20,800	593.8	700	3,446
120	21,050	776.2	700	4,495
121	21,570	815.0	700	4,951
122	20,660	868.8	700	4,499
124	81,190	790.1	700	2,491
125	9,602	376.2	700	1,915
126	9,703	371.7	700	2,291
127	9,813	358.0	700	2,108

TABLE VII

LOCATION OF THERMOCOUPLES

Thermocouple Number	z, inches
2	1.0
3	2.0
4	3.0
5	4.0
6	5.0
7	6.0
8	7.0
9	8.0
10	9.0
11	10.0
12	11.0
13	12.0
14	13.0
15	14.0
16	15.0
17	16.0
18	17.0
19	18.0
20	19.0
21	20.0

z is distance from entrance, i.e., distance from point of power application in direction of flow

APPENDIX III

Sample Calculations

SAMPLE CALCULATIONS

I. Low-Temperature Test Run, 2C

A. Determination of Mass Flow Rate, w

Observations:

Flowmeter pulse count = 48,100 pulses

Meter conditions: t = 99.3F
P = 703 psia

Observation period = 546.24 sec

Flowmeter signal frequency, f = pulses/sec
= (48,100)/(546.24)
= 88.06 cps

Density at meter conditions = 0.4850 gm/cc

Kinematic viscosity at meter = 0.1898 ctks

Ratio of frequency to kinematic viscosity
= (88.06)/(0.1898) = 464 cps/ctks

Meter Constant, K (See Figure 20) = 3302 pulses/gal

Volumetric flow rate = 60 f/k
= 60(88.06)/(3302)
= 1.600 gpm

Mass flow rate of fluid at density = 0.4850 gm/cc
= 388.4 lbm/hr

B. Calculation of Dittus-Boelter h:

Inside tube cross-sectional area, $A_c = \pi D^2/4$
$= \pi(0.02508)^2/4 = 0.000494$ sq.ft.

Bulk fluid temperature (See example calculation described in IIC below) = 114.2F

Pressure = 700 psia

Mass velocity, $G_b = w/A_c = (388.4)/(0.000494)$
$= 7.77 \times 10^5$ lbm/hr.sq.ft.

Thermal conductivity at t_b (24) = 0.05306 Btu/hr.ft.F

Viscosity at t_b (36) = 0.1972 lbm/hr.ft.

Specific heat capacity at t_b (14) = 0.644 Btu/lbm F

Reynolds number = DG_b/μ_b

$= (.002508)(7.77 \times 10^5)/(0.1972)$

$= 9.987 \times 10^4$

Prandtl number = $C_{pb}\mu_b/k_b$

$= (0.644)(0.1972)/(0.05306)$
$= 2.39$

Heat transfer coefficient from Eq. (2)

$$\frac{hD}{k_b} = 0.023\ (Re_b)^{0.8}\ (Pr_b)^{0.4}$$

$$h = \frac{(0.023)(0.05306)(9.987 \times 10^4)^{0.8}(2.39)^{0.4}}{(0.02508)}$$

h = 689 Btu/hr.sq.ft.F

II. Reduction of Test Data for Typical Run

Run No. 62

Observations:

Voltage = 11.07 volts

Average tube wall temperature = 346F

Inlet bulk fluid temperature = 203.57F

Outlet bulk fluid temperature = 217.29F

Pressure at tube entrance = 700 psia

Pressure drop across test section = 0.94 psi

Flowmeter pulse count = 56,640

Meter conditions: t = 145.3F P = 703 psia

Meter observation period = 500.18 sec

A. Calculation of Wall Heat Flux:

Tube resistance (See Figure 17) = 0.030564 ohms

Electrical power dissipated = E^2/Ω
= $(11.07)^2/(0.030564)$
= 13,685 Btu/hr

Tube heat losses (See Figure 19) = 52 Btu/hr

Net rate of heat transferred, $\dot{Q}$ = (13,685 - 52)
= 13,633 Btu/hr

Inside tube surface area, A_i = πDL
= $\pi(0.02508)(21)/12$
= 0.1379 sq.ft.

Wall heat flux = $\dot{Q}/A_i$
= (13,633)/(0.1379)
q_w = 98,870 Btu/hr.sq.ft.

B. Calculation of Overall Heat Balance:

Mass flow rate, w (See example calculation in IA)
= 437.3 lbm/hr

Inlet specific enthalpy at 700 psia = 82.9 Btu/lbm

Specific enthalpy at T_0 and 700 psia = 113.7 Btu/lbm

Pressure correction on exit enthalpy = 0.4 Btu/lbm

Specific enthalpy change, $\Delta\bar{H}_b$ = (113.7 - 82.9 + 0.4)
= 31.2 Btu/lbm

Specific heat input, $\bar{Q}$ = $\dot{Q}/w$
= (13,633)/(437.3)
= 31.18 Btu/lbm

Deviation ($\bar{Q}$ - $\Delta\bar{H}_b$) = 31.2 - 31.2 = 0.0 Btu/lbm

C. Calculation of Bulk Temperature at z = 11.0"

Specific enthalpy change between z = 0 and z = 11.0"
= (11/21) x (overall enthalpy change)
= 0.524 (31.2)
= 16.33 Btu/lbm

Specific enthalpy at z = 11.0" = 82.9 + 16.33
= 99.23 Btu/lbm

Bulk temperature at $\bar{H}$ = 99.23 Btu/lbm and P = 700 psia
= 212.8F

Pressure correction on temperature (See Eq. (45))
= -(0.15)(0.94)(0.524)/(2.5)
= -0.03F (Negligible)

Bulk fluid temperature at z = 11.0" = 212.8F

D. Calculation of Inside Wall Temperature

External wall temperature = 349.8F

Assume temperature drop across tube wall = 12F

Thermal conductivity of Inconel at 344F (arithmetic mean temperature) = 9.58 Btu/hr ft F

Ratio of outside to inside tube radius, ξ
= (0.3585)/(0.301) = 1.191

ξ^2 = (1.191)(1.191) = 1.418

Temperature correction from Eq. (38),

$$t_s - t_w = \frac{-q_w R}{k}\left[\frac{1}{2} - \frac{\xi^2 \ln \xi}{(\xi^2 - 1)}\right]$$

$$= -\frac{(98{,}870)(0.01254)}{958}\left[\frac{1}{2} - \frac{(1.418)\ln(1.191)}{(1.418 - 1)}\right]$$

$t_s - t_w$ = 11.9F

Inside wall temperature = 349.8 - 11.9 = 337.9F

Since the assumed temperature change over the wall thickness is approximately the same as the computed difference, it is not necessary to readjust the thermal conductivity.

E. Calculation of the Heat Transfer Coefficient

$$h = \frac{q_w}{t_w - t_b} = \frac{98{,}870}{337.9 - 212.8} = 790 \text{ Btu/hr.sq.ft.F}$$